GROWTH AND CHARACTERIZATION OF CARBON NANOTUBES BY THERMAL CHEMICAL VAPOR DEPOSITION METHOD

A Thesis Submitted to
The Graduate School of Engineering and Sciences of
İzmir Institute of Technology
In Partial Fulfillment of the Requirements for the Degree of

MASTER OF SCIENCE

in Physics

by
Meral AKSAK

July 2008
İZMİR

We approve the thesis of **Meral AKSAK**

Assist. Prof. Dr. Yusuf SELAMET
Supervisor

Assist. Prof. Dr. Süleyman TARİ
Committee Member

Prof. Dr. Serdar ÖZÇELİK
Committee Member

14 July 2008

Date

Prof. Dr. Durmuş Ali DEMİR
Head of the Physics Department

Prof. Dr. Hasan BÖKE
Dean of the Graduate School of
Engineering and Sciences

ACKNOWLEDGEMENTS

I thank my supervisor Assist Prof Dr Yusuf SELAMET for his invaluable support and encouragement that he provided to me throughout this study.

Also, I thank Assist Prof Dr Süleyman TARİ for his creating a funny atmosphere and positive attitude in his all lectures and for growing our catalyst thin films in his lab whenever we were in need of.

Furthermore, I would like thank Prof Dr Anne Marie BONNOT for the Raman Spectroscopy Measurement at CNRS, Grenoble, FRANCE. I will never forget her for making me motivated, encourage me to go further on this very colorful scientific way, and have positive attitude towards me all the time.

Additionally, I thank Prof Dr Orhan ÖZTÜRK for the XRD measurements and also for his positive attitude all the time. My special thanks also go to the stuff, Duygu, Evrim, Gökhan, and Mine, at the Center for Materials Research of İzmir Institute of Technology, for helping me in performing the analyses of my samples, having a very funny atmosphere during my Master's thesis, and also for their humanity and helpfulness'. Furthermore, I thankfully acknowledge TUBITAK for providing me scholarship and project funding (TUBITAK TBAG-105T462) during my thesis. Moreover, I am very thankful to my lab mates and friends at İzmir Institute of Technology.

Last but not least, I express my sincere gratitude to my family for their ceaseless financial support, motivation, and positive attitudes in all aspects and in all parts of my life, all the time. I am sincerely grateful to them for urging me to do science, where I am extremely happy!

ABSTRACT

GROWTH AND CHARACTERIZATION OF CARBON NANOTUBES BY THERMAL CHEMICAL VAPOR DEPOSITION METHOD

This thesis work is focused on producing carbon nanotubes (CNTs) by methane gas thermal chemical vapor deposition method on very thin Cobalt, Iron, and Nickel catalyst thin films deposited onto SiO_2/Si substrates by DC magnetron sputtering. This thesis is also devoted to understanding some parameters affecting the growth of CNTs; such as catalyst material, temperature, and catalyst layer thickness effects.

In this study, CNT growth was performed on directly Si substrates, which was observed that the growth was too difficult and requiring very high temperatures. Hence, very thin catalyst films were deposited on SiO_2/Si substrates, and the CNT growth was observed.

The temperature effect was also examined. When the growth temperature was increased, the average diameters of the CNTs were decreased up to a critical temperature, but after this point the average diameter of CNTs were increased. This effect was studied systematically by utilizing Fe and Co catalyst thin films and with the help of Raman spectroscopy and Scanning Electron Microscopy results.

Catalyst thickness effect was also examined. For this aim, Ni catalyst thin films with three different thicknesses; 0.7 nm, 1.4 nm, and 6 nm, were utilized. It was observed that CNTs were grown well on 0.7 and 1.4 nm thick Ni films, while there was a little growth on 6 nm thick Ni film. The roughness analysis of 0.7 nm and 1.4 nm thick Ni films were also done. Some of as-grown CNTs were also examined by X-ray diffraction method, and the results were compared one another.

ÖZET

KARBON NANOTÜPLERİN TERMAL KİMYASAL BUHAR BİRİKTİRME YÖNTEMİ İLE BÜYÜTÜLMESİ VE KARAKTERİZASYONU

Bu tez çalışması, karbon nanotüplerin metan gazı termal kimyasal buhar biriktirme yöntemi ile, doğru akım mıknatıssal saçtırma tekniği ile silikon dioksit kaplanmış silikon alttaşlari üzerine kaplanan Kobalt, Demir ve Nikel çok ince kataliz filmlerinin üzerinde büyütülmesine odaklanmıştır. Bu çalışma, ayrıca karbon nanotüplerin büyümesini etkileyen bazı parametreleri, örneğin sıcaklığın etkisi, kataliz materyalinin ve kataliz ince filmin kalınlığının etkilerini anlamaya adanmıştır.

Bu çalışmada karbon nanotüp büyümesi direkt olarak sadece silikon filmler üzerinde denenmiştir; silikon üzerinde büyümenin çok zor olduğu ve çok yüksek sıcaklıklar gerektiği gözlenmiştir. Bu nedenle silikondioksit/silikon alttaşı üzerine kataliz tabakaları kaplandı ve yüksek sıcaklıklarda büyüme gözlendi.

Ayrıca, sıcaklığın etkisi araştırıldı. Büyüme sıcaklığı arttırıldığında, karbon nanotüplerin ortalama yarıçaplarının kritik bir sıcaklık değerine kadar azaldığı ancak kritik bir değerden sonra arttığı gözlendi. Sıcaklığın etkisi, Fe ve Co kataliz filmleri ve Raman spektroskopisi ile yüzey taramalı mikroskop sonuçları kullanılarak sistematik olarak çalışıldı.

Kataliz kalınlığının karbon nanotüp büyümesi üzerindeki etkisi de incelendi. Bu amaç için, farklı kalınlıklardaki, 0.7 nm, 1.4 nm ve 6 nm, Nikel ince filmler kullanıldı. Elde edilen sonuçlardan, karbon nanotüplerin 0.7 nm ve 1.4 nm kalınlıklardaki filmler üzerinde, 6 nm kalınlıktakine kıyasla daha iyi büyüdüğü gözlendi. Ayrıca, 0.7 ve 1.4 nm kalınlıktaki Nikel filmlerin yüzeylerinin pürüzlülüğü ölçüldü. Bazı karbon nanotüpler X-ışını kırınımıyla da incelenip, elde edilen sonuçlar diğer sonuçlarla kıyaslandı.

Dedicated to;

My lovely family

For being always with me!

TABLE OF CONTENTS

LIST OF FIGURES

LIST OF TABLES

CHAPTER 1

INTRODUCTION

The discovery of carbon nanotubes (CNTs) was not only a giant leap for science but also an inspiring step to open an incredible era for many research areas worldwide. Many scientists have been trying to figure out the unknown properties of these gorgeous nanostructures which are about to be in power of nanoscience, as they are being used in chemistry, electronics, physics, medicine, engineering, etc.

A CNT is a nanometer-sized hexagonal graphene structures which shows very high chemical stability (Heer and Ugrate 1993) and very large current density (10^9 A/cm^2) (Dresselhaus, et al. 2001). CNTs have many distinct properties over the other conventional nano-materials for their extraordinary mechanical, electrical, structural, and optical properties (Dresselhaus, et al. 2001). They are believed to be one of the strongest and stiffest materials with respect to their tensile strength and elastic modulus since they have covalently bonded carbon atoms within their graphitic structures (Dresselhaus, et al. 2001, Baughman, et al. 2002).

The CNTs are classified mainly as single-walled carbon nanotubes (SWNTs) and multi-walled carbon nanotubes (MWNTs) (Dresselhaus, et al. 2001). It was shown that an (n, m) CNT is metallic if n=m or (n-m) = 3i, where *i* is an integer and n and m defining the CNT structure ($C=n\hat{a}_1+m\hat{a}_2$, C is chirality vector) (Thostenson, et al. 2001). Moreover, SWNTs also come in three types as armchair, zigzag, and chiral nanotubes (Ivchenko and Spivak 2002). The most distinct and well known property of them is that the CNTs can be either metallic or semiconducting depending on their structures (Saito, et al. 1992, Baughman, et al. 2002). All armchair nanotubes are metallic nanotubes while zigzag nanotubes are to be either semiconducting or metallic (Saito, et al. 1992).

All CNTs are very good electrical conductors along their tube axis, exhibiting a property known as "ballistic conduction," and very good insulators perpendicular to the tube axis (Roth and Carroll 2004, Ivchenko and Spivak 2002). It is predicted that the CNTs will be able to transmit up to 6000 $W\cdot m^{-1}\cdot K^{-1}$ at room temperature; compare to copper, which only transmits 385 $W\cdot m^{-1}\cdot K^{-1}$ (Yi, et al. 1999, Hone, et al. 1999). The temperature stability of CNTs is estimated to be up to 2800°C in vacuum and about 750°C in air (Begtrup, et al. 2007). The differences in conducting properties are caused

by the molecular structure which results in a different band structure and thus a different band gap (Avouris 2002, Baughman, et al. 2002).

Additionally, CNTs are the stiffest and the strongest fibers known; a SWNT can be up to 100 times stronger than that of steel this is due to C-C bonds (Baughman, et al. 2002). The Young's modulus of SWNT is up to 1 TPa, which is 5 times greater than steel (230 GPa) while the density is only 1.3 g/cm^3 (Saito, et al. 1992). They have high tensile strength (130 GPa bundled strength) high chemical storage capacity, e.g. hydrogen storage (Kajiura, et al. 2003).

Furthermore, they have high aspect ratio; the ratio is the word defining the ratio of their length to diameter (Dresselhaus, et al. 2001). There has been a huge interest to create longer CNTs since the longer have the better application ability. In the early years making CNTs length longer and longer was a big target, the only aim was to increase the length from micrometer scale to millimeter. Nowadays, scientists are likely to reach the centimeter scale growth on regular basis.

Zhu and his co-workers reported that they produced very long single-walled CNTs by catalytic chemical vapor deposition method using ferrocene as catalyst and hydrogen as carrier gas; they also compared the CNTs diameter with human hair. The length of these carbon nanotubes was 20 cm and 10 cm, these strands generally have a diameter of 0.3 mm, which is larger than a human hair (Zhu, et al. 2002). In order to realize large scale CNT applications they are to be grown in large quantities. In this aspect, CVD gives the best hope to come over this problem compare to other method. This method had been reported for preparation of various carbon materials such as carbon fibers and MWCNTs with high yield and at large scale (Journet and Barnier 1998).

The as-grown CNTs can have different morphology or structure, although they are grown with the same parameters. These kinds of facts are still being investigated. For example, Lee and his co-workers from Republic of Korea investigated the temperature effect on the growth of CNTs; they observed that as the temperature increased the as grown CNTs were formed with larger size, low density, and broad diameter distribution (Lee, et al. 2001).

On the other hand, another group, Makris and his co-workers from Italy observed that low temperature corresponded to thicker, shorter and less curved CNTs, whereas higher temperature resulted in CNTs with thinner diameter and greater length (Makris, et al. 2005).

Also, the best catalyst material type has been investigated by different groups. The results of choosing the best catalyst metal are not that much of controversial. The groups share the same idea that Fe, Ni, and Co nanoparticles have very good performance since carbon has very high solubility in these metals at high temperatures (Dai 2002).

The main objective of this thesis is to optimize the parameters of CNTs produced by methane thermal chemical vapor deposition and to investigate main parameters affecting the growth of CNTs, such as catalyst, temperature, and catalyst thickness effects. This thesis is composed of six chapters. Chapter 2 gives a background on CNTs, their discovery, types, structure, and growth methods along with growth mechanisms. Chapter 3 is devoted to a brief literature survey on catalysts and sputtering process. Chapter 4 is the experimental section, consisting of catalyst preparation steps by sputtering and CNT growth steps by Thermal Chemical Vapor Deposition method (TCVD), and the characterization techniques used for the analyses of as-grown CNTs. Chapter 5 presents the results and discussions part. Finally, the conclusions are given in Chapter 6.

CHAPTER 2

CARBON NANOTUBES

2.1. Discovery

CNTs are considered as graphene sheets rolled up into cylinders with diameters as small as 0.4 nm (Guan, et al. 2008, Dai 2002). Although CNTs attracted significant attention worldwide in 1991 because of its very small size, actually, their observation is not so new (Iijima 1991, Monthioux and Kuznetsov 2006). There have been so many investigations for a long time concerning with the exact date of the first observation of CNTs so as to make clear who should be credited with the discovery of CNTs (Monthioux and Kuznetsov 2006). It was shown that a type of MWNTs were firstly observed by Russian researchers Radushkevich and Lukyanovich in 1952, which unfortunately did not draw much attention owing to the fact that the article related to this experiment was in Russian, therefore, access to this article was limited during the Cold War (Monthioux and Kuznetsov 2006, Radushkevich and Lukyanovich 1952). The same Russian researchers also examined the samples under transmission electron microscope and showed that there were some kinds of nearly 50 nm in diameter tubes made of carbon; related images are depicted in the Figure 2.1.a and Figure 2.1.b.

In 1976, there was another paper published by Oberlin and his co-workers in (Oberlin, et al. 1976); these researchers grew some carbon nanofibers with diameters of on the order of nanometer scale using vapor growth technique; the related image is seen in Figure 2.1.c, which depicts some kinds of single or double walled carbon nanotubes.

At that time, there was a new discovery of buckminsterfullerene (C_{60}) observed by Smalley, Kroto and his co-workers in 1985 and they were awarded by Nobel Prize in Chemistry in 1997 (Kroto, et al. 1985). The discovery of fullerenes opened a new era in the field of nanotechnology and this work was also an inspiration for researchers working on nanoscience worldwide. A Japanese electron microscopist Sumio Iijima was one of them who inspired of the discovery of fullerenes. He kept on his experiments in order to observe some other allotropes of fullerenes, and luckily he came across with some tiny tubes along with fullerene like structures (Iijima 1991). He did the experiments in ‘Arc-Discharge Evaporation’ system by varying electrical current

between two graphite electrodes and then collecting the growth structures in the sooty atmosphere (Iijima 1991). The MWNTs grown by Iijima are depicted in Figure 2.2.

Two years later, Iijima along with his co-workers and Bethune and his co-workers produced independently the first SWNTs nearly at the same time (Iijima and Ichihashi 1993, Bethune, et al. 1993), the related images are depicted in Figure 2.3.a and Figure 2.3.b, respectively. The production of these SWNTs was succeeded in adding some iron metal onto either anode or cathode or both electrodes (Ando, et al. 2004).

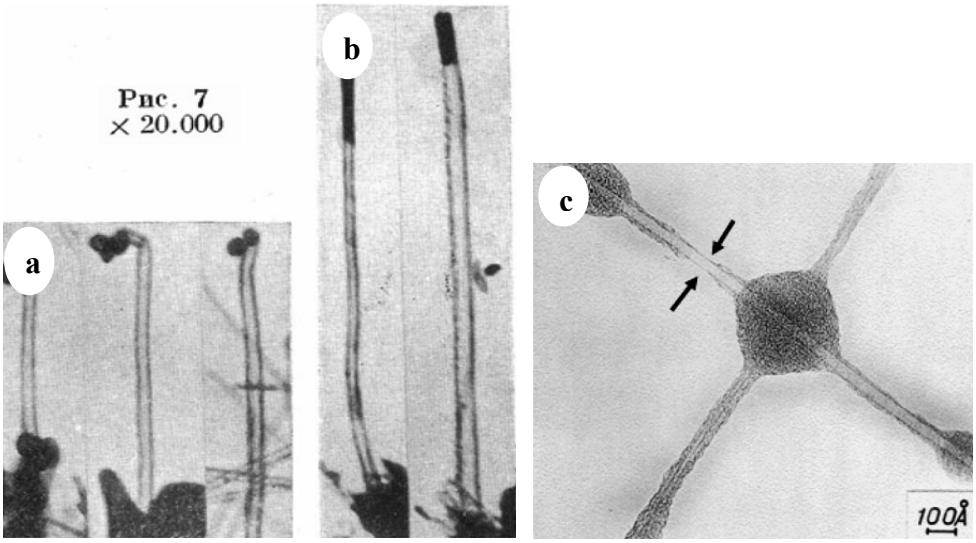

Figure 2.1. a) and b) TEM images of CNTs (Source: Radushkevich and Lukyanovich 1952), c) TEM image of SW- or DWNTs (Source: Oberlin, et al. 1976)

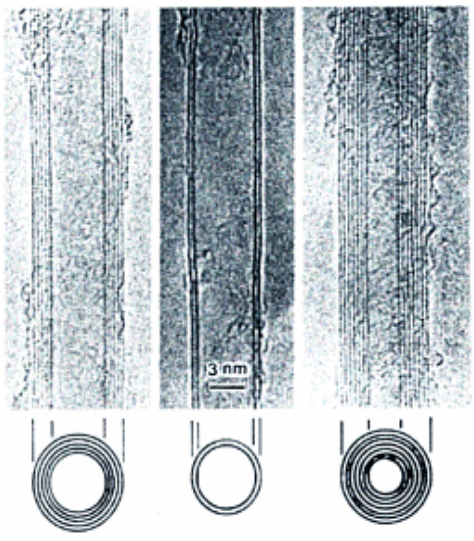

Figure 2.2. TEM images of MWNTs observed by Sumio Iijima
(Source: Iijima 1991)

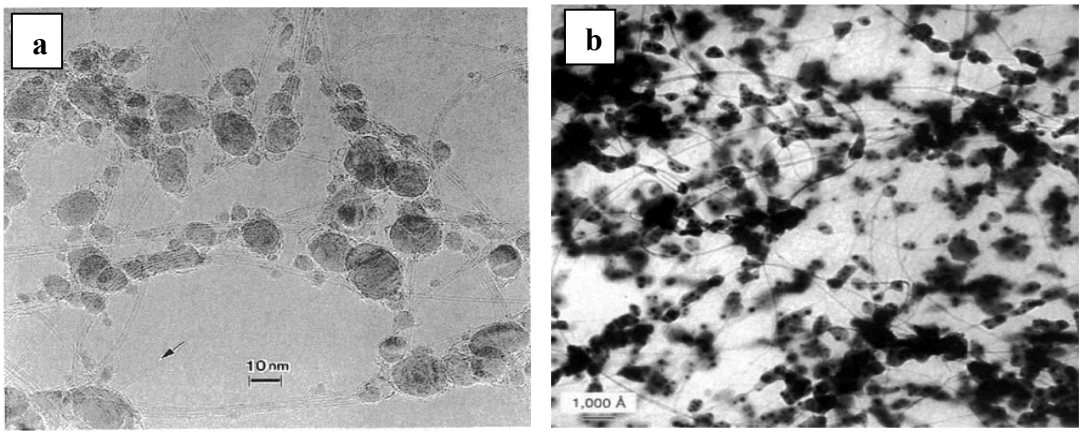

Figure 2.3. TEM images of, a) the bundles of SWNTs (Source: Iijima and Ichihashi 1993), b) the web-like structures of SWNTs (Source: Bethune, et al. 1993)

2.2. Types of Carbon Nanotubes

A CNT is named according to the number of graphite layers; if there is only one sheet rolled into a cylinder, it is called as SWNT; whereas there are more than one layer, the carbon nanotubes are then called MWNTs (Dresselhaus, et al. 2001).

2.2.1. Single-Walled Carbon Nanotubes

A SWNT is separated among other types of nanotubes by its having only one wall with the diameter of ranging from 0.4 nm (Guan, et al. 2008) to 5 nm as well as having high aspect ratio (Dai 2002). SWNTs are mostly preferred nanotube type due to their perfect mechanical, electrical, and structural properties as well as their having less defects with compared to MWCNTs, which is relatively easier to control the structure of SWNTs than MWNTs (Dai 2002).

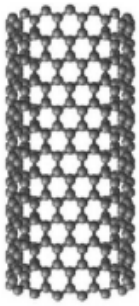

Figure 2.4. An illustration of a SWNT

(Source: Dresselhaus, et al. 2003)

2.2.2. Multi-Walled Carbon Nanotubes

A MWNT is considered as coaxial cylindrical stacks of graphene sheets whose graphene walls are parallel to the central axis (Merkoci 2006) with an interlayer spacing of 0.34 nm (Dresselhaus, et al. 2001), a diameter of on the order of 5-100 nm and their lengths up to μm or even cm range (Dai 2002). All MWNTs are metallic NTs.

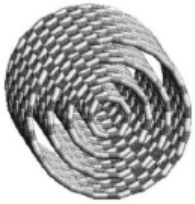

Figure 2.5. An illustration of a MWNT

(Source: Dresselhaus, et al. 2003)

2.3. Structure of Carbon Nanotubes

A CNT is considered as a graphene sheet rolled into a cylindrical shape being one dimensional structure as well as having an excellent axial symmetry (Saito, et al. 1998). The important fact to be remembered that the type of a CNT is identified by the rolling direction of the hexagons which are the six-membered carbon rings (Dresselhaus, et al. 2001). There are two important parameters to control the type of a CNT, one of which is the chiral angle (Θ) while the other one is chiral vector (C_h) (Reich, et al. 2004). The chiral angle, Θ, being the angle between C_h and $\hat{a}_1$ is measured relative to the direction defined by $\hat{a}_1$ (Rotkin and Subramoney 2005). These two parameters are clearly seen in Figure 2.6.

The structure of a CNT is well identified by the vector called chiral vector, $C_h=n\hat{a}_1+m\hat{a}_2$, where $\hat{a}_1$ and $\hat{a}_2$ are unit vectors, or so-called graphite lattice vectors, and n and m are the integers (Dresselhaus, et al. 2001), which are crucially important to decide whether a CNT is zigzag, chiral or an armchair nanotube (Dresselhaus, et al. 2001); therefore the chiral vector behaves like the fingerprints of CNTs as for their defining the structural character of the CNTs. As it is clearly seen from the Figure 2.6, the structure of a SWNT is defined by the OA vector being perpendicular to the NT axis, is of crucial importance in defining the structure of NTs. OA vector is the chiral vector of CNT (Dresselhaus, et al. 2001); the chiral vector is shown clearly in Equation 2.1:

$$OA= C_h=n\hat{a}_1+m\hat{a}_2 \qquad (2.1)$$

To form the CNT, the cell which is seen in Figure 2.6, is rolled up into a cylinder so that O meets with A and B meets with B', and the two ends are capped with half of a fullerene molecule; the unit cell of a CNT is bounded by OAB'B (Dai 2002). Different types of CNTs have different values of n and m; that is to say these nanotubes do have different diameters which are also meaning that the nanotubes are to be in different structures. The chiral vector thus forms the circumference of the circular cross-section of the carbon nanotube, and different values of n and m lead to different nanotube structures with different chiral vectors (Saito, et al. 1998). Depending on the tube chirality, the electrical properties of the CNTs differ from one another; that is to say that CNTs can be metallic or semiconducting; if n-m=3p, where p is an integer, the CNTs are metallic; while n-m≠3p, the CNTs are semiconducting (Ivchenko and Spivak 2002).

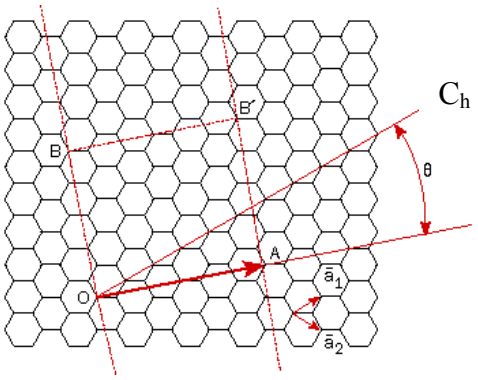

Figure 2.6. The unrolled, two-dimensional, honeycomb lattice of a CNT

(Source: Saito, et al. 1998)

CNTs are formed with three different structures (Saito, et al. 1998). If the atoms around the circumference are in arm-chair shapes, they are called 'armchair' NTs with (n=m) integers, which always show metallic character; while if the atoms are arranged in zigzag shapes, the CNTs are 'zigzag' NTs with (m, 0) indices showing either metallic or semiconducting behavior; if atoms are shaped in spiral shapes in the axial direction, they are called 'chiral' NTs (Dai 2002, Dresselhaus, et al. 2001). The classifications of CNTs are depicted in Figure 2.7.

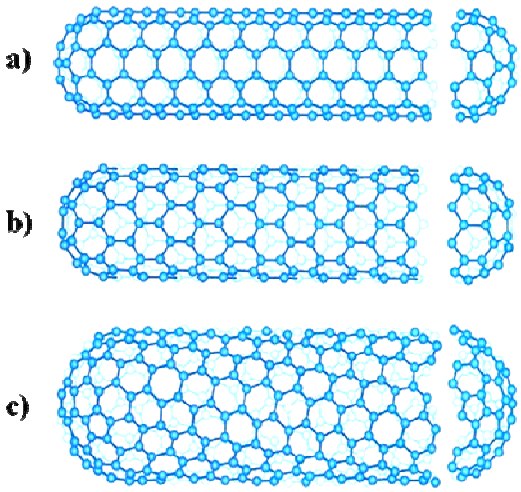

Figure 2.7. Classification of CNTs, a) Arm-chair, b) Zig-zag, c) Chiral CNTs

(Source: Dresselhaus, et al. 2001)

2.4. Carbon Nanotube Synthesis Methods

There have been three common CNT growth techniques one of which is arc-discharge method (Bethune, et al. 1993); while the other two are called laser ablation method (Thess, et al. 1996) and chemical vapor deposition method (Dai 2002, Ebbesen 1994). The results obtained by these three methods differ from each other since each has its own growth dynamics and each method has its own advantages and disadvantages. These three growth methods are briefly explained below.

2.4.1. Arc-Discharge Method:

Arc-Discharge method is the most common and the oldest one used in the growth of CNTs worldwide. This technique depends on applying a low voltage (20-40 V) and a DC current (nearly 50-100 Å) between cathode and anode in order to produce a discharge (Iijima 1991). Applying current between the electrodes causes anode to vaporize and condense either on the walls or the cathode surface of which the observations showed that the deposit on the cathode surface is NTs. The temperature of the plasma reaches at very high temperatures (nearly ~4000°C) which must be enough to vaporize the anode which is made of graphite.

The evaporation of the carbon from the anode is generally done in a helium atmosphere (Popov 2004) and large scale synthesis of MWCNTs was achieved in Helium atmosphere (Colbert, et al 1994). It has been observed that the CNTs can also be grown in the liquid nitrogen atmosphere or in water (Alexandrou, et al. 2004). A typical illustration of an arc-discharge apparatus is depicted in Figure 2.8. In arc-discharge experiment, the distance must be adjustable so as to keep the constant distance between two electrodes (Harris 2007). By this method, CNTs are produced at relatively high temperatures over the other growth methods but with very high yield per unit time and with very well crystallized CNTs.

SWNTs are produced with the help of catalyst material (such as Fe, Co, Ni, etc) (Bethune, et al. 1993, Iijima and Ichihashi 1993); however there is no limitation for MWCNT growth since MWNTs can be produced without catalyst (Dai 2002).

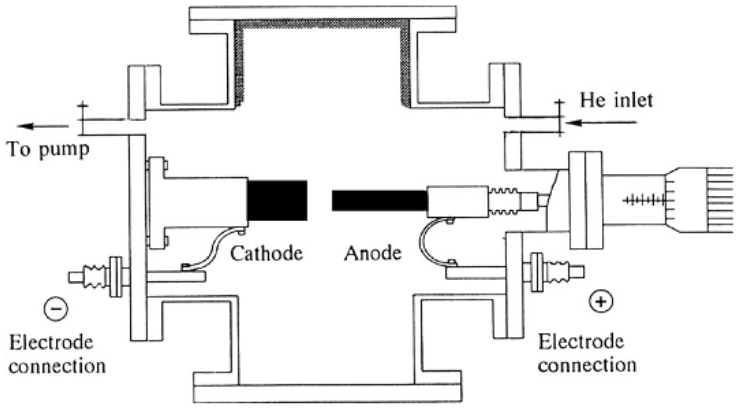

Figure 2.8. Schematic illustration of an arc-discharge apparatus
(Source: Harris 2007)

2.4.2. Laser-Ablation Method

The laser ablation method was used firstly for the growth of fullerenes (C_{60}) by Richard Smalley group in 1985 (Kroto, et al. 1985). In 1995 the group of Guo used this method to produce CNTs (Guo, et al. 1995). A typical illustration of a laser-ablation method is depicted in Figure 2.9.

This method is performed generally at very high temperatures, nearly at 2500°C in an argon or helium gas environment kept at 500 Torr pressure in a temperature controlled furnace where a graphite target is placed in the middle of the quartz tube (Harris 2007). Since the energy density of lasers is much higher than that of other vaporization devices, the laser is suitable for materials with a high melting temperature, such as carbon (Ando, et al. 2004). After vaporizing the target, the vaporized carbon is carried to the cupper collector which is cooled by a water cooling system and deposits the carbon on the top surface of this copper collector (Harris 2007).

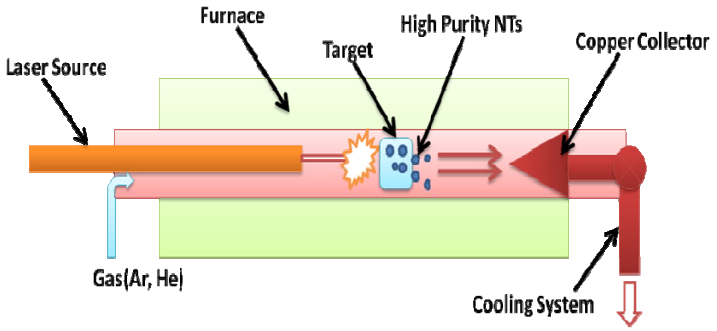

Figure 2.9. Schematic illustration of a laser ablation method
(Source: Guo, et al. 1995, Journet and Barnier 1998)

If the target used in this method is made of pure graphite target, i.e. there is no catalyst substance deposited on the target, MWNTs are likely to be produced (Guo, et al. 1995); otherwise it is possible to produce SWNTs by adding catalyst particles into the graphite target (Ando, et al. 2004). An image of SWNTs grown by laser-ablation method is seen in Figure 2.10.

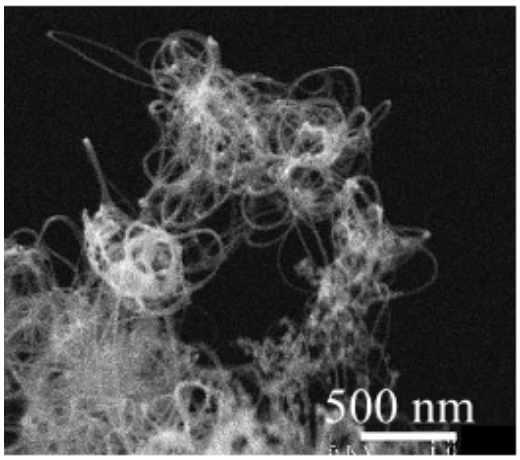

Figure 2.10. The SWNTs grown by laser ablation method
(Source: Thess, et al. 1996)

2.4.3. Chemical Vapor Deposition Method

The utilization of CVD technique is not new for it was used firstly in order to grow carbon fibers and carbon filaments a long time ago (Walker, et al. 1959). In 1993, Yacaman and his co-workers successfully grew CNTs by CVD technique; they

performed the growth of CNTs with acetylene as a hydrocarbon gas and iron particles as catalyst at 700°C (Yacaman, et al. 1993).

Since then, CVD has been preferred growth method for CNTs since it has many advantages over the other techniques, such as high scalability, having an advantage of accommodating more than one sample at one time at the desired temperature and relatively low growth temperature with compared to the other methods (Reich, et al. 2004). What is more, it is possible to control the length, diameter, and alignment of the CNTs to a certain degree by adjustment some of the growth parameters. The typical hydrocarbon gases used in CVD are acetylene, ethylene, methane, etc (Kong, et al. 1998, Moisala, et al. 2003). A typical schematic illustration of chemical vapor deposition method is depicted in Figure 2.11.

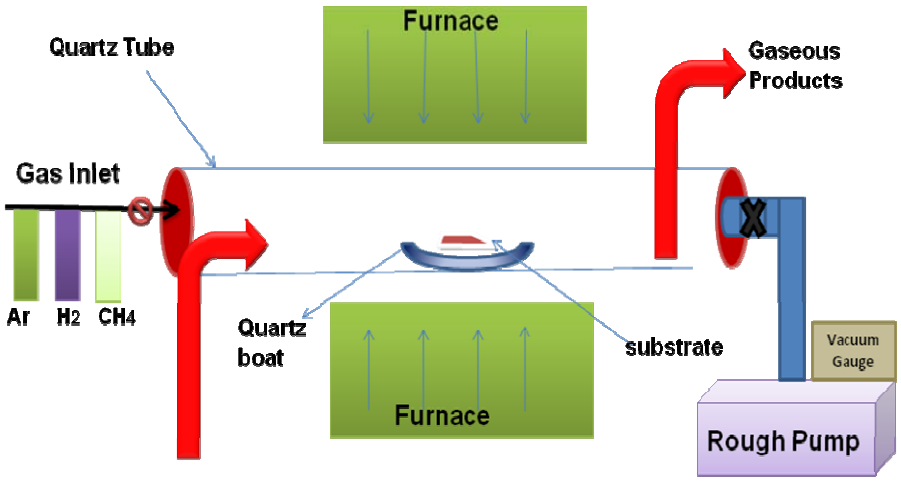

Figure 2.11. A schematic illustration of a CVD System
(Source: Journet and Barnier 1998)

The main steps followed in the growth of CNTs by CVD method are; first, insertion the substrate onto which CNTs to be grown; second, heating the system to the desired temperature in an inert gas environment; third, sending an etching gas such as hydrogen, nitrogen, or ammonium so as to form the catalyst nanoparticles; fourth, sending a hydrocarbon gas into the system then decompose this hydrocarbon gas on the catalyst nanoparticles. Furthermore, CNTs growth over the catalyst nanoparticles, and finally, cooling the system down to room temperature in an inert gas atmosphere. This

kind of CVD method is generally called catalytic CVD or TCVD method. The first CNTs grown by CVD are seen in Figure 2.12. The CNTs seen in Figure 2.12 were produced over $Fe/SiO_2/Si$ catalyst in the decomposition of C_2H_2 at 700°C (Ivanov, et al. 1994).

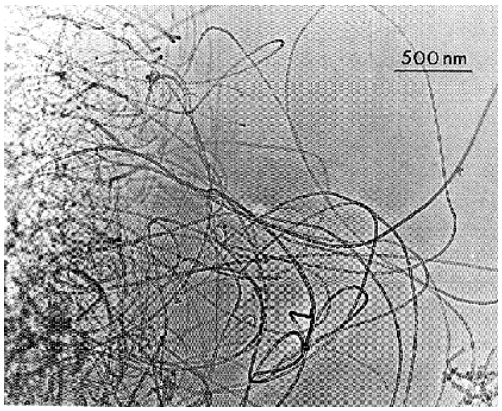

Figure 2.12. TEM image of CNTs produced by TCVD
(Source: Ivanov, et al. 1994)

2.5. The Growth Mechanism of Carbon Nanotubes

The growth mechanism of CNTs is not fully known owing to the fact that the growth dynamics of the CNTs have not been completely understood (Ando, et al. 2004, Lee, et al. 2001). Some studies proposed several growth models. The first growth mechanism suggested for the growth of carbon fibers by Bakers et al (Baker, et al. 1972, Baker and Harris 1978, Baker, et al. 1972), which has helped many researchers to have some idea about the growth mechanism of the CNTs. This growth model is illustrated in Figure 2.13.

According to this growth model, firstly, it is essential to grow some nucleation sites, so-called catalyst nanoparticles (shown in the 1st step of Figure 2.13). Carbon goes into the these catalyst nucleation sites, then diffuses down to these nucleation sites (shown in the 2nd step of Figure 2.13), and furthermore the precipitation of carbon at the rear of the particle builds up a deposit of carbon which forces the particle away from the support (seen in the 3rd step of Figure 2.13) (Baker and Harris 1978). Once the catalyst particle is supersaturated with carbon, it extrudes out the excess carbon in the form of a tube (Kukovitsky, et al. 2002).

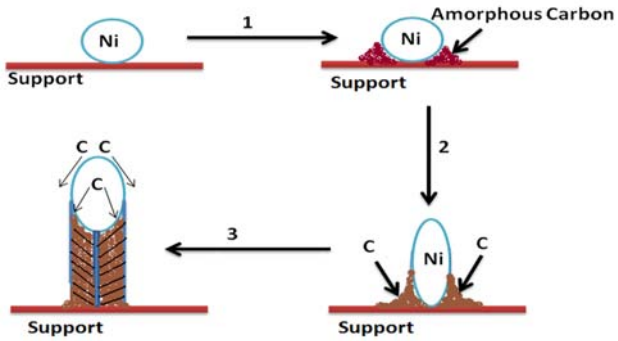

Figure 2.13. An illustration of CNT growth steps
(Source: Baker and Harris 1978)

CNTs can grow in either base (root) growth or tip growth mechanisms. These mechanisms are named whether the catalyst nanoparticles are at the tip of the CNTs or at the bottom side (Saito, et al. 1994). If there is a strong interaction between the catalyst and substrate it is called base growth model; or else it is tip growth if the catalyst nanoparticle is lifted up by the growth of CNTs (Dresselhaus, et al. 2001). Formation of SWNTs or MWNTs is mostly governed by the size of the catalyst particle (Lee, et al. 2001, Kukovitsky, et al. 2002) that is to say, if the catalyst particle size is a few nanometers, SWNTs would form, whereas particles of a few tens of nanometers wide would favor MWNT formation (Ando, et al. 2004).

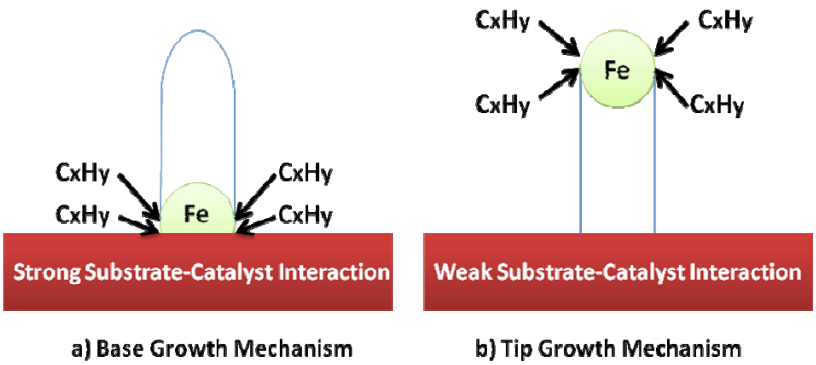

Figure 2.14. An illustration of CNT growth mechanisms, a) Base-Growth, b) Tip-Growth mechanism (Source: Ando, et al. 2004)

CHAPTER III

ON CATALYSTS

The catalyst material has been considered one of the indispensible parameters affecting the growth of CNT in an important way since it is the substance responsible for having either SWNTs or MWNTs and either with the tip-growth or base growth mechanisms. In the first section of this chapter, a brief literature survey on catalyst materials will be given. The second section covers a brief explanation on sputtering process which was used for deposition of the catalyst materials throughout this thesis work.

3.1. A Short Literature Survey on Catalyst Materials

There have been a variety of parameters affecting the growth of CNTs; catalyst material is one of the most important parameters affecting the CNT growth. Numerous articles in the literature point out that the catalyst is absolutely required material so as to have the CNT in relatively short time with well defined shape and structure (Laurent, et al. 1998, Ando, et al. 2004, Lee, et al. 2002). Much research has been done into which catalyst gives the best result for the CNT growth by utilizing the elements in the periodic table (Deck and Vecchio 2006, Qingwen, et al. 2002, Laurent, et al. 1998).

The common catalyst materials used for the CNT growth have been Fe, Co, and Ni in the literature. It has been observed that it is possible to grow both MWNTs and SWNTs by using Fe, Co, and Ni (Deck and Vecchio 2006, Dupuis 2005, Laurent, et al. 1998).

When iron-based catalyst was used, many research groups observed SWNTs (Dupuis 2005**,** Cheng, et al. 1998, Li, et al. 2001, Cheung, et al. 2002, Nikolaev, et al. 1999, Zhu, et al. 2002, Hayashi, et al. 2003, Hongo, et al. 2002, Zhang, et al. 2002, Satishkumar, et al. 1998) and also MWNTs were observed by utilizing Fe **(**Dupuis 2005, Kukovecz, et al. 2000, Pérez-Cabero, et al. 2003, Sen, et al. 1997, Ermakova, et al. 1997, Pan, et al. 1999, Ivanov, et al. 1994, Venegoni, et al. 2002, Hernadi, et al. 1996, Fonseca, et al. 1996, Cui, et al. 2000, Cho, et al. 2002, Duesberg, et al. 2003).

Mostly MWNTs were observed when Co-based catalyst was utilized (Dupuis 2005**,** Ivanov, et al. 1994, Hernadi, et al. 1996, Fonseca, et al. 1996, Ago, et al. 2000, Hsu, et al. 2002, Ago, et al. 2003), a few groups observed SWNTs when Co-based catalyst (Dupuis 2005**,** Satishkumar, et al. 1998, Marty, et al. 2002, Colomer, et al. 1999, Colomer, et al. 2000).

When Ni catalyst was used, groups observed mostly MWNTs (Dupuis 2005**,** Ivanov, et al. 1994, Yudasaka, et al. 1995, Teo, et al. 2001, Ren, et al. 1998, Klinke, et al. 2001, Choi, et al. 2000, Huang, et al. 1998, Jiao and Seraphin 2000, Kukovitsky, et al. 2002, Siegal, et al. 2002, Wright, et al. 2003, Yudasaka, et al. 1997) and very rarely SWNTs were observed by utilizing Ni catalyst material (Dupuis 2005**,** Colomer, et al. 1999, Colomer, et al. 2000, Seidel, et al. 2004).

It was investigated that for Ni, Co, and Fe, carbon has a finite solubility in these metals at high temperatures, which leads to the formation of metal-carbon solid state solutions (Dai, 2002, Park, et al. 2002). It was also observed that the ability for transition metals to bond with carbon atoms increases with the number of unfilled d-orbital, for metals such as Al, Au, and Pd have no d-vacancies and negligible affinity for carbon (Arthur and Cho 1973). Metals with few d-vacancies such as Ni, Co, and Fe exhibit finite solubility for carbon in certain temperature ranges. 3d and 4d metals with many d-vacancies such as Ti and Nb can form strong chemical bonds with carbon and thus highly stable carbide compounds (Arthur and Cho 1973).

There was a very good systematic study done on catalyst materials in the periodic table (Deck and Vecchio 2006). It was observed that the three transition metals, Fe, Co, and Ni, are considered the best among others because of the fact that these all have high carbon solubility (~ 0.5-1.0 wt %) at high temperatures (800-900°C) in the solid solution (Deck and Vecchio 2006, Laurent, et al. 1998). It was also considered that in the solid solution there were stable carbides (iron carbide, nickel carbide, and cobalt carbide) (Laurent, et al. 1998, Deck and Vecchio 2006). At the solid solution solubility limit with iron, stable carbide (Fe_3C) is produced (Deck and Vecchio 2006). When Fe_3C solid is saturated with carbon (at 6.67 wt% C), graphite forms and, when nanoscale catalyst particles are used, this graphite will be produced with a NT structure. Co_3C, Co_2C, and Ni_3C form immediately following saturation of carbon in the solid solution, and additional carbon diffuses into the catalyst, graphite precipitates out, forming CNT (Deck and Vecchio 2006).

It was also observed that in the Cu, Zn, Gd, and Cd systems studied, the solubility limit of carbon in the metals was extremely low; for example 0.0001 wt %C in Cu at 1100°C which is above the melting point of Cu (Hansen 1958, Deck and Vecchio 2006). Carbon cannot diffuse in significant quantitites into the nanoscale catalyst particles, and therefore these particles cannot act as nucleation sites for the formation of CNT (Deck and Vecchio 2006).

Also, the performances of those three catalyst materials was investigated according to their growth rate of CNTs which was on the order of Ni>Co>Fe (Lee, et al. 2002). The average diameter of CNTs follows the sequence of Fe>Co>Ni catalysts (Lee, et al. 2002). The peculiar ability of these metals was suggested to relate to the catalytic activity for decomposition of carbon precursors, the formation of meta-stable carbides, the diffusion of carbons, and the formation of graphitic sheets (Kiang 2000).

Furthermore, it was also investigated that if the elements in the periodic table are categorized into which is very good or not, it has been reached the conclusion that d-electron transition metals are so very successful catalyst materials among all in the periodic table (Richardson 1989).

As for the alkali and alkaline s-metals, they tend to revert too easily to ionic states under catalytic conditions which are not suitable for the growth of CNTs (Richardson 1989). Rare earth f-metals likewise are too difficult to produce and too reactive to remain in the metallic state, there is no example of successful catalysis with rare earth metal (Richardson 1989). Moving from right to left across the periodic table means less d-electron is available to fill the bands of energies corresponding to collectivized d-orbitals. Levels are filled successively until the Fermi is reached (Richardson 1989).

The key to obtaining high yields of pure CNTs is achieving hydrocarbon decomposition on catalyst site alone and avoiding spontaneous pyrolysis. It is remarkable that the transition metals have proven to be efficient catalyst not only in CVD but also in arc-discharge and laser ablation methods (Richardson 1989). Transition metals such as Fe, Ni, and Co are frequently used catalysts in the growth of CNTs. In addition, Sc, Ti, V, Cr, Mn, Y, Zr, Nb, Mo, Hf, Ta, W, Re or a combination of them are also used for this purpose (Deck and Vecchio 2006).

3.2. Sputtering Process

There have been numerous techniques for depositing thin films in today's technological applications; among them the sputtering method is widely used one which is a Physical Vapor Deposition (PVD). It has several advantages over the other conventional thin film deposition techniques, such as good surface uniformity, growth on substrates, and its cost effectiveness (Seshan 2002). The catalyst materials used in this thesis work were deposited by DC magnetron sputtering process.

Sputtering relies on the transfer of linear momentum and kinetic energy from the incident particle to the surface atoms impact on the surface or near-surface atoms of the solid with sufficient energy to break the bonds and dislodge the atoms. In this process, atoms removed from the solid target are called the sputtered atoms (Seshan 2002). A magnetron uses a static magnetic field configured at the cathode location. The magnetic field is located parallel to the cathode surface. Secondary electrons which are emitted from the cathode due to ion bombardment are constrained by this magnetic field to move in a direction perpendicular to both the electric field (normal to the surface) and the magnetic field (Seshan 2002).

These secondary electrons are trapped in a region close to the cathode. Eventually, they lose their kinetic energy due to collisions with gas atoms (ionization) or with other electrons (electron heating) and the net result is dense plasma in this drift ring. Visually this is quite easy to see in magnetron sputtering system. The drift path light up dramatically and there is no question the density is much higher in this region. The location of this ring is also known as the etch track because the erosion of the cathode is highest here and deep groves can be eroded onto the cathode. Ions which are made in the drift region have a high probability of hitting the cathode which is close by. This results in even more production of secondary electrons and eventually extremely dense plasma (Seshan 2002).

CHAPTER 4

EXPERIMENTAL

This chapter is devoted to the experimental processes used throughout this thesis work. The first section of this chapter is focused on the catalyst film deposition processby DC magnetron sputtering. Second section offers a brief explanation about the thermal CVD, third section covers the main growth steps of CNTs by TCVD method, and final section is focused on the characterization techniques (SEM, AFM, XRD, and Raman Spectroscopy) used for characterization of as-grown CNTs throughout this thesis work.

4.1. Catalyst Film Deposition by DC Magnetron Sputtering Process

In this study, the DC magnetron sputtering method was utilized so as to deposit the catalyst films (Fe, Co, Ni) onto the SiO_2/Si substrates. The sputtering system used for depositing the catalyst thin films for the growth of CNTs is AJA ATC Orion 5 UHV sputtering system based in Magnetism Lab, IYTE. This system is controlled by a computer and reaches very high vacuum levels. It is composed of four 2-inch magnetron heads including a substrate holder which is able to rotate at different speeds so as to have a uniform deposition, a heater, and a load-lock with a magnetic arm with a cylindrical stainless steel chamber. The targets are bonded to a water cooled copper carrier, ensuring both electrical and thermal contact.

The chamber base pressure can reach about 5×10^{-6} Torr with the help of turbo molecular pump before the catalyst film growth. In the chamber, above the substrate there are two halogen lamps so as to heat the substrate at different temperatures varied from room temperature to nearly 850°C.

The thickness of the thin film is measured by an in-situ thickness monitor. The distance between substrate and target was kept at 7 cm. The parameters used for the deposition of Fe, Co, and Ni thin films are given in Table 4.1.

Table 4.1. Growth conditions of catalyst thin films for DC magnetron sputtering

Material Name	Power (Watt)	P (mTorr)	d (cm)	t_{growth}	t (nm)
CoSiO5	20	3	7	5 min	~3.5
FeSiO7	40	3	7	2 min	~1.2
NiSiO1	20	3	7	1 min	~0.7
NiSiO2	20	3	7	2 min	~1.4
NiSiO3	20	3	7	10 min	~6

4.2. Thermal Chemical Vapor Deposition Process

The TCVD system used for the CNT growth is composed of two parts; one of the parts is a Lindberg/Blue M 1200C Split Hinge Tube Furnace in horizontal use and the other one is an independent controller (Model CC58114C Controller). An image of the TCVD system used throughout this study is depicted in Figure 4.1. The hinge tube furnace also involves a quartz tube (~1200 mm in length, 1 inch diameter) and a quartz boat. The quartz boat is used for a bed for the samples onto which the CNTs were grown. The quatz boat and the samples are depicted in Figure 4.2.a and Figure 4.2.b, respectively.

The quartz boat onto which the substrates were accommodated is placed in the middle of the furnace; since there is an isothermal area. The upper temperature limit of the hinge furnace is 1200°C; which is lower than the melting temperature of quartz, and hence the maximum temperature limit was restricted to 1000°C throughout this thesis study.

Figure 4.1. The TCVD system based in Physics Department, CNL Lab, IYTE

Figure 4.2. a) Quartz boat, b) Some thin films used for CNT growth

The reactor is heated by a resistance furnace. The flow value of the gases sent into the system is read via mass flow controllers. Before the CNT growth, the system should be brought to the vacuum level in an inert gas ambient, generally argon (Ar) gas is used for this purpose as a carrier gas, which is responsible for carrying the foreign atoms and by products before and after the CNT growth processes so as to have a clean atmosphere. Then the furnace is set to the desired temperature before the CNT growth, and the temperature is increased in an Ar ambient.

After the desired temperature is reached, etching or dilution gases are sent into the system so as to form the catalyst nanoparticles. After etching away the catalyst film and forming the catalyst nanoparticles, a hydrocarbon gas is sent into the system at the desired temperature and pressure; afterwards, the CNT growth starts by sending the hydrocarbon gas. In this study, three gases were utilized; methane as a carbon precursor gas, hydrogen gas as an etchant gas and diluent gas, and argon gas was used to have a

vacuum and an inert gas atmosphere along with having a role carrying the by-products both after and before the growth.

4.3. CNT Growth Process by TCVD

In all experiments, it was tried to reach low vacuum with the help of a diaphragm valve which is connected to mechanical pump and quartz tube before the CNT growth which was between 2-15 Torr, and the pressure was kept at ~350 Torr during the CNT growth.

Furthermore, after having reached the desired vacuum, the temperature was set to the expected reaction temperature at an increase rate of 28°C/min, and then the system was heated in an Ar gas ambient until the desired growth temperature was reached. After the temperature was stabilized, H_2 gas was sent with the Ar gas, and then the Ar was switched off and H_2 gas was sent alone as an etchant gas for five minutes with the flow rate of 120 sccm.

Methane (CH_4) gas was utilized for it is the most stable hydrocarbon gas against self-decomposition at high temperatures, and the catalytic decomposition of CH_4 by the transition metal catalyst particles is the dominant process in SWNT growth (Dai 2002). For the CNT growth, CH_4 and H_2 gas mixture was sent into the system, with the flow rate of 100 sccm and 50 sccm, respectively. The growth was carried on 30 minutes in all experiments. After 30 minutes, first, CH_4 gas was switched off and after some time H_2 gas was turned off, as well; and the system was set to room temperature in Ar gas ambient. The cooling process was continued nearly 6 hours. All the growth conditions are listed in the Table 4.2.

Table 4.2. Growth conditions of CNTs for TCVD method

Sample Name	Increase Rate (°C/min)	Ar (sccm)	CH_4:H_2 (sccm)	$P_{initial}$ (Torr)	P_{growth} (Torr)	Time (min)	T (°C)
CoSiO5CNT32	28	120	100:50	4.7	~350	30	850
CoSiO5CNT33	28	120	100:50	5.1	~350	30	875
CoSiO5CNT37	28	120	100:50	15.9	~350	30	900
CoSiO5CNT38	28	120	100:50	10.7	~350	30	925
CoSiO5CNT39	28	120	100:50	4.8	~350	30	950
CoSiO5CNT49	28	120	100:50	4.4	~350	30	975
FeSiO7CNT51	28	120	100:50	3.4	~350	30	700
FeSiO7CNT52	28	120	100:50	3.4	~350	30	750
FeSiO7CNT53	28	120	100:50	3.8	~350	30	800
FeSiO7CNT54	28	120	100:50	3.7	~350	30	850
FeSiO7CNT55	28	120	100:50	3.6	~350	30	900
FeSiO7CNT57	28	120	100:50	3.9	~350	30	925
FeSiO7CNT58	28	120	100:50	4.0	~350	30	950
FeSiO7CNT59	28	120	100:50	3.8	~350	30	975
FeSiO7CNT60	28	120	100:50	3.7	~350	30	1000
NiSiO1CNT75	28	120	100:50	2.4	~350	30	850
NiSiO2CNT76	28	120	100:50	2.4	~350	30	850
NiSiO3CNT77	28	120	100:50	2.4	~350	30	850
NiSiO1CNT78	28	120	100:50	2.2	~350	30	900
NiSiO2CNT79	28	120	100:50	2.2	~350	30	900
NiSiO3CNT80	28	120	100:50	2.2	~350	30	900
NiSiO1CNT81	28	120	100:50	2.0	~350	30	950
NiSiO2CNT82	28	120	100:50	2.0	~350	30	950
NiSiO3CNT83	28	120	100:50	2.0	~350	30	950
Si53	28	120	100:50	3.8	~350	30	800
Si54	28	120	100:50	3.7	~350	30	850
Si55	28	120	100:50	3.6	~350	30	900
Si56	28	120	100:50	3.2	~350	30	950

4.4. Characterization Techniques

It is nothing without any characterization techniques to analyze the experimental results. The tools used for examining the samples give absolutely crucial properties about the samples. Different characterization techniques were used to examine the as-grown CNTs; namely Scanning Electron Microscopy (SEM), Atomic Force Microscopy (AFM), X-Ray Diffraction Method (XRD), and Raman Spectroscopy,

4.4.1. Scanning Electron Microscopy

Scanning electron microscopy (SEM) is one of the main surface analysis instruments, which is the simplest and most accessible technique. It is also the first characterization technique used for analyzing the CNTs worldwide although it has some limitations while examining the surface of the sample. It cannot measure the diameter of the CNTs precisely, but roughly. Apart from this, its resolution is restricted; therefore after some magnification it is likely to neither see the images totally nor give the exact information about the wall numbers of CNTs. Even though it has both advantages and some drawbacks, it is the first characterization technique to be used in analyzing the CNTs.

As to mention about its working principle, the SEM depends on sending highly focused electrons on the sample in order to scan the surface of the sample in a vacuum chamber. While these focused electrons scan the surface of the sample, it is an unavoidable fact that there have other electrons emitted and scattered along with forming X-rays, which are then collected by different detectors. The outputs collected by detectors give invaluable information about the sample. In SEM, there are three main images to be observed: secondary electron images, backscattered electron images, and elemental X-rays maps. Secondary electron images can be obtained on all materials identifying surface features, on most instruments, to a practical limit of ~100 nm. Despite the considerable depth of penetration of the incident primary electron beam (e.g. 0.5-5μm), re-emitted electrons (as secondary and backscattered electrons) comes from the mean depths of 50 nm-5 μm depending on the density of the material. Hence, this technique is sensitive to the near-surface region. Scanning the beam over the surface minimizes the surface damage and surface charging. Backscattered electron

images can give contrast based on the average atomic number of the region or phase examined. Topographic images obtained by combining different backscattered electron images can reveal detail of pits and protrusions, precipitates and altered regions on the surface (O'Connor, et al. 2003). The SEM utilized throughout this thesis work was Philips XL 30S, FEG.

4.4.2. Atomic Force Microscopy

Atomic Force Microscopy (AFM) is crucially important for providing significant information about the topography and structural properties of thin films by measuring the forces between the surface and tip interaction, such as Van der Waals, electrostatic, frictional, and magnetic forces.

According to the working principle of the AFM, the tip which is stuck on the tip of a cantilever and generally made of silicon carbide scans the surface of a sample by different modes, principally in two modes, tapping mode (non-contact) mode and contact mode. The tapping mode is generally the desired one due to it's not touching the sample surface and not damaging the surface, while in the contact mode, there is an interaction between the tip and the surface atoms leading to remove the atoms from their places and scratch the surface of the material. Additionally, the tapping mode gives better image resolution compared to other modes.

The AFM used throughout this study was Multimode SPM, Nanoscope-IV Digital Instrument with an ultra sharp tip performed with non-contact mode, at the Material Research Center, IYTE.

4.4.3. X-Ray Diffraction Method

X-ray diffraction (XRD) method is very powerful tool for analyzing the structural properties of different phases of not only thin films but also powder samples while giving the exact information about the structure of the crystalline material, such as stress, grain size, phase composition, crystal orientation and defects. It is also possible to get more information about whether there are any other materials in the sample.

If a monochromatic X-ray beam falls on such a crystal, each atomic plane reflects the beam. Each separate reflected beam interacts with other reflected beams. If the beams are not in phase, they destroy each other and emerge from the crystal. The net result is a diffraction pattern of reinforced beams from many planes. It is the atomic planes that are important in X-ray diffraction.

The XRD is based on the Bragg equation which describes the condition for constructive interference for X-rays scattering from atomic planes of a crystal (Feldman and Mayer 1986). The condition may be satisfied by varying λ or varying orientation of a single crystal. In thin films the distribution of crystallite orientations is nearly continuous. Diffraction occurs from crystallites which happen to be oriented at the angle to satisfy Bragg equation (Feldman and Mayer 1986).

The XRD utilized in this thesis was Philips X'pert Pro X-ray diffractometer with Cu-K_α X ray source λ=1.5418 Å.

4.4.4. Raman Spectroscopy

Raman spectroscopy is of crucial importance for better understanding of not only the structure but also the type of CNTs as well as providing crucial information about the quality of CNTs whether as-grown CNTs have defects or they are well-graphitized. This tool also gives the information about the type of CNTs whether they have armchair nanotubes, zigzag, or chiral structures.

It uses scattering of a light within a material to characterize its structure. The basic principle of Raman Spectroscopy is that when a beam of light traverses transparent sample a small fraction of the light scattered in the directions other than that of the incoming beam (Shanov, et al. 2006). Most of this scattered light is of unchanged wavelength. However a small part has wavelengths different from the incident light and its presence is a result of the Raman Effect (Shanov, et al. 2006). Micro-Raman spectroscopy is used for characterization of CNTs with a typical excitation wavelength laser.

The characteristic spectrum of SWCNT exhibits 3 main zones at low (100-250 cm^{-1}), intermediate (300-1300 cm^{-1}), and high (1500-1600 cm^{-1}) frequencies (Colomer, et al. 2000, Maultzsch, et al. 2002), these bands can be produced by the presence of

other carbon forms like MWCNTs and amorphous carbon (Cheng, et al. 1998). These three zones have also other names, as Radial Breathing Modes (RBM), D (disordered)-modes, and G (Graphite)-modes, respectively (Qingwen, et al. 2002).

The RBM is of crucial important while having an idea about the diameter distribution of SWNTs. This mode is very sensitive to the diameter of SWNTs and generally seen for up to 3 nm (Dresselhaus, et al. 2002).

D-band is observed around 1300 cm^{-1} (for excitation with He-Ne laser with the wavelength of 632 nm) or at 1350 cm^{-1} when using Ar ion 488 nm laser (Eklund, et al. 1995, Reich, et al. 2004). The D peak is related to the presence of defects. The high intensity of D-band is associated with high defects in density. The other band is called the G-peak at about 1580 cm^{-1}, which is associated with the in-pale vibrations of the graphene sheet (Eklund, et al. 1995). G-band is very important due to the fact that it gives very good information about the character of SWNTs (Dresselhaus, et al. 2002).

Ratios of D-peak to the G peak have been used as an indicator of the amount of disorder within CNTs. A small I_D/I_G ratio, typically in the range of 0.1 - 0.2, indicates that the defect level in the atomic carbon structure is low, which suggests reasonable crystalline quality. In other words, a high ratio between the G band and D band peak intensities indicates that the CNTs are of high purity (Eklund, et al. 1995, Dresselhaus, et al. 2002).

The G mode can be decomposed in one main peak with a shoulder (Rao, et al. 1997, Dresselhaus, et al. 2002). This shoulder is more important in the case of SWCNT, because it gives the information about the CNTs whether they are semiconducting or metallic CNTs (Rotkin and Subramoney 2005, Reich, et al. 2004). The typical Raman spectra are shown in Figure 4.3.

As it is depicted in the Figure 4.3 that the G-band has also a G^- band at lower frequencies with an asymmetric and broad shape, which is associated with metallic character of the nanotube. If the shoulder is narrow with a tangential rear shape then the nanotubes show semiconductor behavior (Dresselhaus, et al. 2002).

The Raman Spectrometer used for characterization of our CNTs is a Lab-Ram Infinity from Dilor with a wavelength of 633nm, the incident radiation is a laser He-Ne, , focused onto the substrate through an objective of a microscope. The probe area is about 1-2μm^2 and the laser power is in the order of 1mW. The Raman images were taken at CNRS, Grenoble, France.

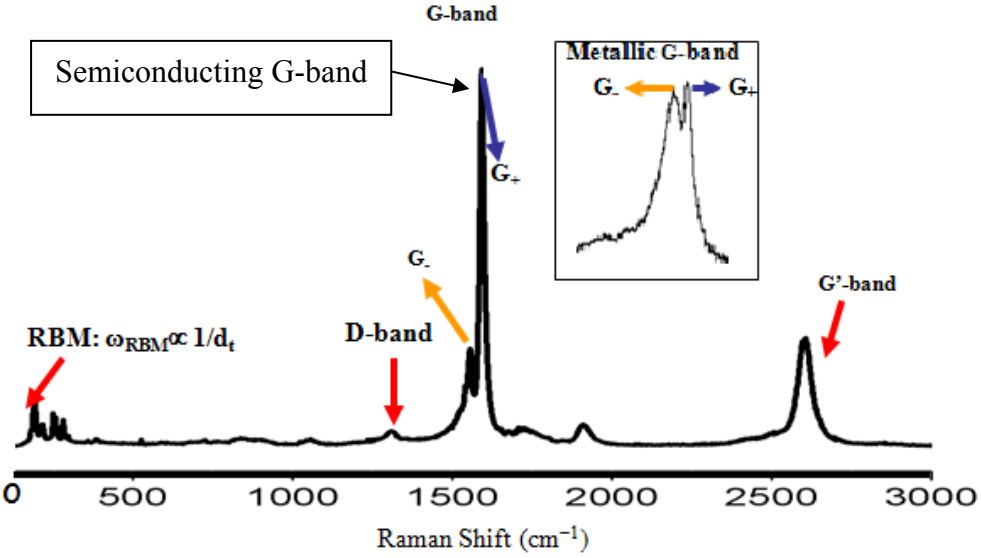

Figure 4.3. Raman spectra showing the main peaks and the characters of SWNTs (Source: Dresselhaus, et al. 2002)

CHAPTER 5

RESULTS AND DISCUSSION

This chapter is devoted to the results and discussions of the experiments. The first section of this chapter is focused on understanding of the catalyst and temperature effect on the CNT growth, of which the experiments were performed directly on Si substrates and also catalyst (Fe, Co, Ni) deposited SiO_2/Si substrates. The second section examines the catalyst layer thickness effect on the growth of CNTs. Furthermore, the results were compared one another by examining SEM, AFM, X-ray Diffraction (XRD), and Raman Spectroscopy results, which will be given respectively.

5.1. SEM Results

5.1.1. Catalyst and Temperature Effects on the CNT Growth

5.1.1.1. Growth on Bare Si Substrates

The regular growth was directly applied on bare Si substrates, which did not have any catalyst layer, named as Si53, Si54, Si55, and Si56. The results were examined to observe whether there was any CNTs growth or not by utilizing only Si substrates. The experiments were performed at 800°C, 850°C, 900°C, and 950°C, for Si53, Si54, Si55, and Si56, respectively. The other all parameters were kept constant in order to observe only the temperature effect on CNT growth.

Figure 5.1.a. illustrates that CNT growth conditions were directly performed on Si substrates at 800°C, which also demonstrates that there was no tubular structure on the surface of the Si substrate; the Si nanoparticles were covered amorphous carbon. It was observed that the temperature was not enough for carbon atoms to be dissolved in the Si nanopparticles then the temperature was increased. Figure 5.1.b. depicts that CNT growth was directly performed at 850°C, it is seen from the image that the nanoparticles were covered with amorphous carbon, but there was still no CNT structures. It was decided to keep going further to higher temperature, and Si55 sample was utilized for this aim at 900°C, the result is depicted in Figure 5.1.c, whose Si nanoparticles were covered with fully amorphous carbon. The CNT growth was performed again directly

on the Si substrates but this time at 950°C, depicted in Figure 5.1.d. It was observed that the sample surface was covered with mainly amorphous carbon like a cloud. From the SEM pictures, there seemed some tubular-like structures but one or two, not too many.

The reason for this is that the solubility of carbon in Si nanoparticles is too low, and required very high temperatures on the range of 1560 - 2900°C (Taylor, et al. 1993, Scace and Slack 1959). Moreover, carbon precipitation in Si appeared to be an extremely difficult process at these temperature values used in the experiments. Since the hinge furnace system had a maximum temperature range of the system, 1200°C, the temperature was not exceeded 1000°C.

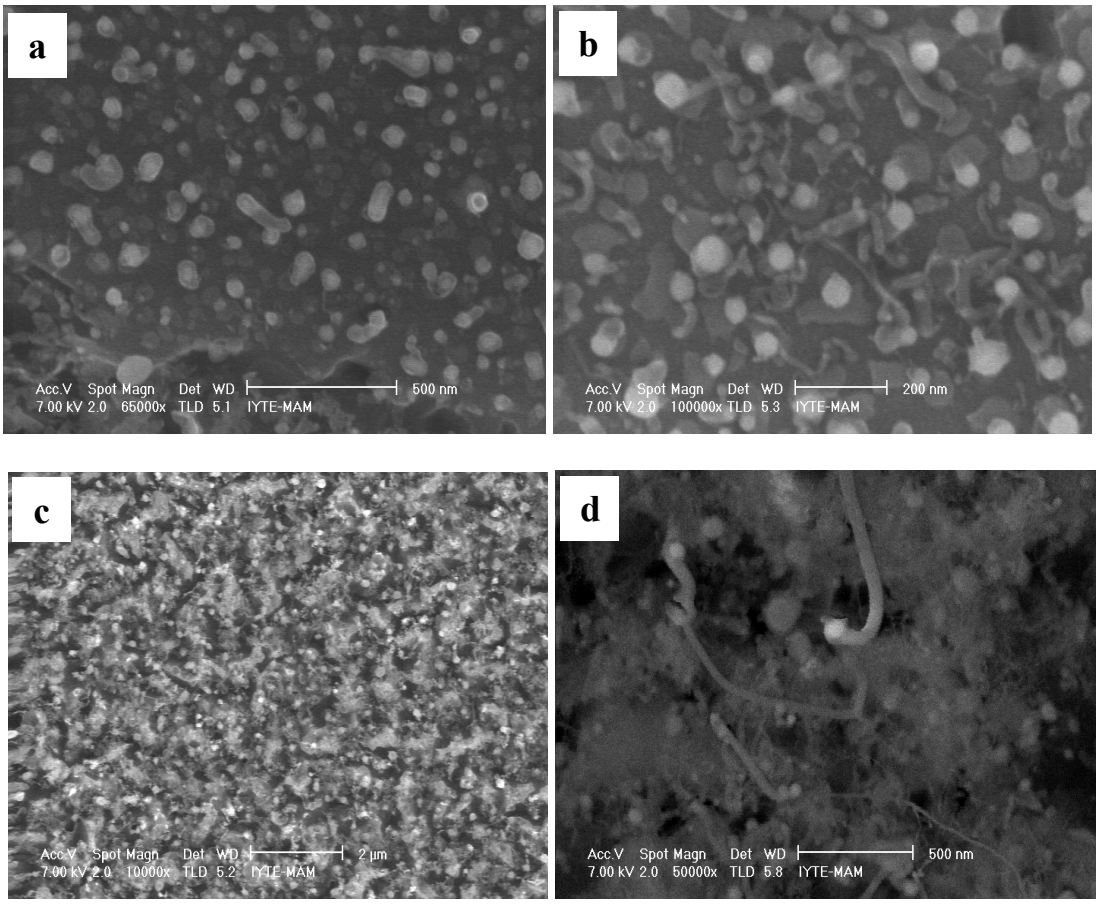

Figure 5.1. SEM micrographs of, a) Si53 at 800°C, b) Si54 at 850°C, c) Si55 at 900°C, d) Si56 at 950°C

5.1.1.2. CNT Growth on Fe/SiO_2/Si Samples

CNT growth was then applied on Fe-deposited SiO_2/Si thin films. The Fe catalyst film thickness was measured from the in-situ thickness monitor at around ~1.2 nm. The experiments were performed at different temperatures keeping all the other parameters constant in order to observe only the temperature effect on the CNT growth. Firstly, it was tried to observe the temperature value at which Fe catalyst nanoparticles were grown, the average diameters of these Fe catalyst nanoparticles were measured from SEM.

Even though CH_4 was sent through the reaction zone as a hydrocarbon gas, at three different temperatures, 700, 750, 800°C, there was not any CNT growth. This is due to the fact that carbon has low solubility at these temperatures; in other words, these temperatures were not enough for the Fe catalyst nanoparticles to solve carbon atoms.

The catalyst nanoparticles grown at 700°C, 750°C, 800°C are depicted in Figure 5.2.a, Figure 5.2.b, and Figure 5.2.c; respectively. The average diameters were measured approximately as 35.67 nm for the Fe catalyst nanoparticles grown at 700°C, depicted in Figure 5.2.a. While the average diameters of the Fe catalyst nanoparticles grown at 750°C and 800°C were measured as 30.19 nm and 28.31 nm, respectively. The results are given in Table 5.1.

It was observed that when the temperature was increased, the average diameter of catalyst nanoparticles was decreased. When the temperature was increased, the rate of hydrogen gas of etching away the catalyst thin film was also increased, which leaded to finer and smaller catalyst nanoparticles.

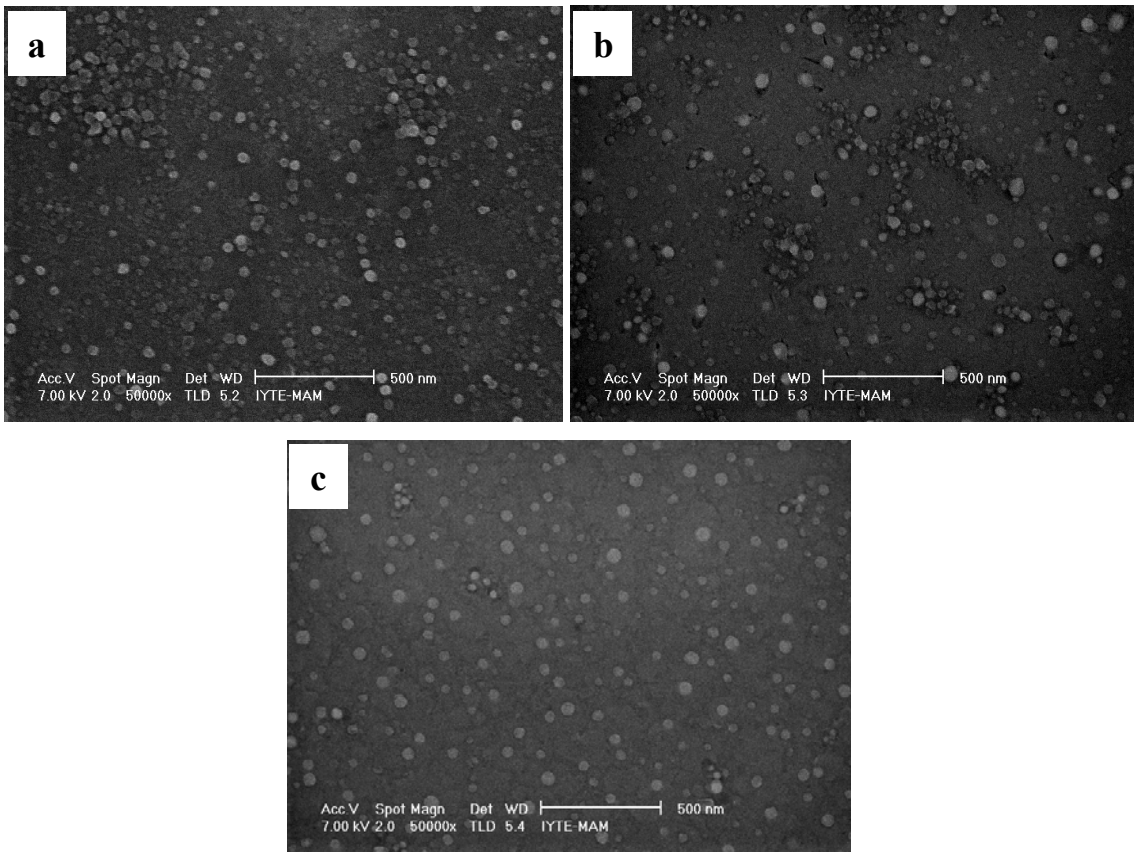

Figure 5.2. SEM micrographs of Fe nanoparticles produced at, a) 700°C on Fe51/SiO_2/Si, b) 750°C on Fe52/SiO_2/Si, c) 800°C on Fe53/SiO_2/Si

Table 5.1. Average diameters of Fe nanoparticles at different temperatures

Sample	Temperature (°C)	Average Diameter (nm)
FeSiO7CNT51	700	35.67
FeSiO7CNT52	750	30.19
FeSiO7CNT53	800	28.31

When the temperature was increased from 800°C to 850°C, the catalyst nanoparticles were encapsulated by amorphous carbon. The related images are depicted in Figure 5.3, taken with two different magnifications of 20000 and 100000, respectively. As it is seen from the Figure 5.3, nearly all Fe catalyst nanoparticles were

covered with amorphous carbon. This was due to the fact that the solubility of carbon was still very low at 850°C, which leaded the catalyst nanoparticles to be encapsulating by amorphous carbon provided that the temperature was not enough for the catalyst nanoparticles to be active for the CNT growth (Snoeck, et al. 1997).

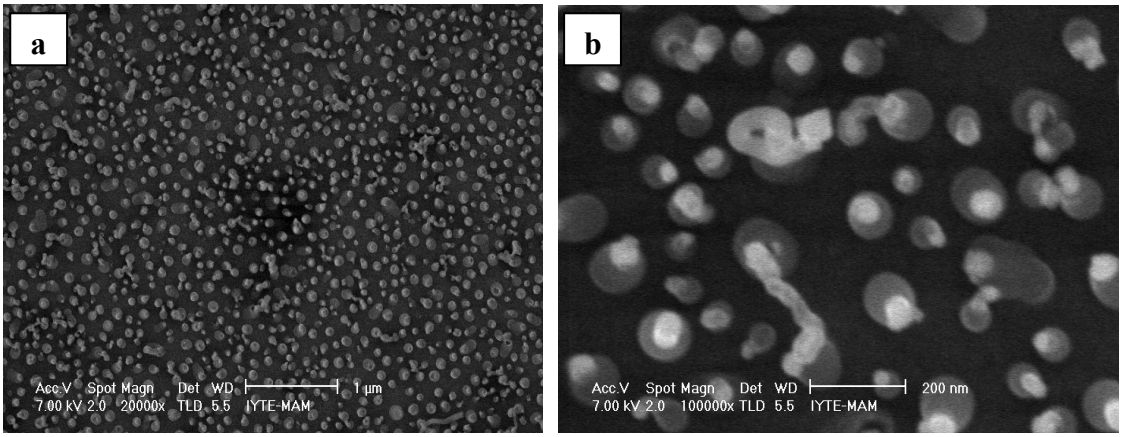

Figure 5.3. SEM micrographs of Fe54/SiO_2/Si nanoparticles covered with amorphous carbon at 850°C, a) magnification: 20000X, b) magnification: 100000X

The temperature was then increased from 850°C to 900°C; which is depicted in Figure 5.4.a. The CNTs seen in Figure 5.4.a were curved and woven each other, it was deemed that they consisted of defects within themselves; some pentagons or some carbon atoms might not be in its place so there could be some vacancy, leaded to CNTs to be curved. The average diameters of these as-grown CNTs were measured from SEM approximately 20.02 nm.

Then the temperature was increased from 900°C to 925°C, and the result is depicted in Figure 5.4.b. as it is seen from the Figure 5.4.b, the as-grown carbon nanotubes were not well-aligned, but curved, short, and bulky. The average diameters of these as-grown CNTs were approximately 14.43 nm. It is also clearly seen from both images that some parts of the as-grown CNTs are brighter than the other parts. And also the brighter parts are at the tip of the as-grown CNTs, meaning that the CNTs were grown according to tip-growth mechanism.

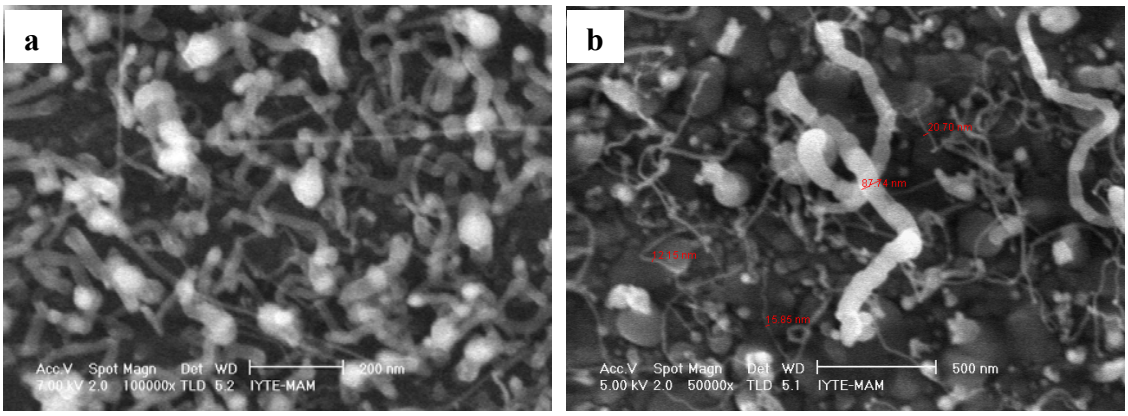

Figure 5.4. SEM micrographs of as-grown CNTs on, a) Fe55/SiO_2/Si at 900°C, b) Fe57/SiO_2/Si at 925°C

Furthermore, the temperature was increased from 925°C to 950°C, and the related image is depicted in Figure 5.5.a. It is seen from the image that the as-grown CNTs were thinner and longer than those grown at lower temperatures of 900°C, and 925°C. The average diameter of CNTs grown at 950°C was measured approximately 13.86 nm. These CNTs were grown according to tip growth mechanism, since the catalyst nanoparticles are seen at the tips of the CNTs.

At high temperature the CNTs were formed with thinner diameter, and greater length, otherwise they were with shorter length and thicker diameter. It is also seen from the images (Figure 5.4.a, Figure 5.4.b, and Figure 5.5.a) that at low temperatures, the CNTs were less curved with, however at high temperatures CNTs were woven each other. Furthermore, it was observed that the length was also increasing with increasing the temperature.

Then, the temperature was increased to 975°C, related image is shown in Figure 5.5.b, the average diameter of those as-grown CNTs were measured nearly 18.12 nm. This result was really interesting due to the fact that the average diameter was expected to be decreased, but here the average diameter was increased with increasing the temperature. When the temperature was increased to 1000°C, the average diameters of CNTs were measured at around 38.83 nm. The as-grown CNTs were depicted in Figure 5.5.c. The results are given in Table 5.2.

Although the temperature was increased, it was observed that the lengths of CNTs were increased but the average diameters of as-grown CNTs were increased.

Graphite layers are occurred when the carbon concentration inside the metallic nanoparticle exceeds supersaturation. When the carbon precipitates out, the surface tension of the catalyst particle is increased, and the dissolution of carbon starts again. Then the thickening of the nanotubes occurs layer by layer (Ruemmeli, et al. 2005).

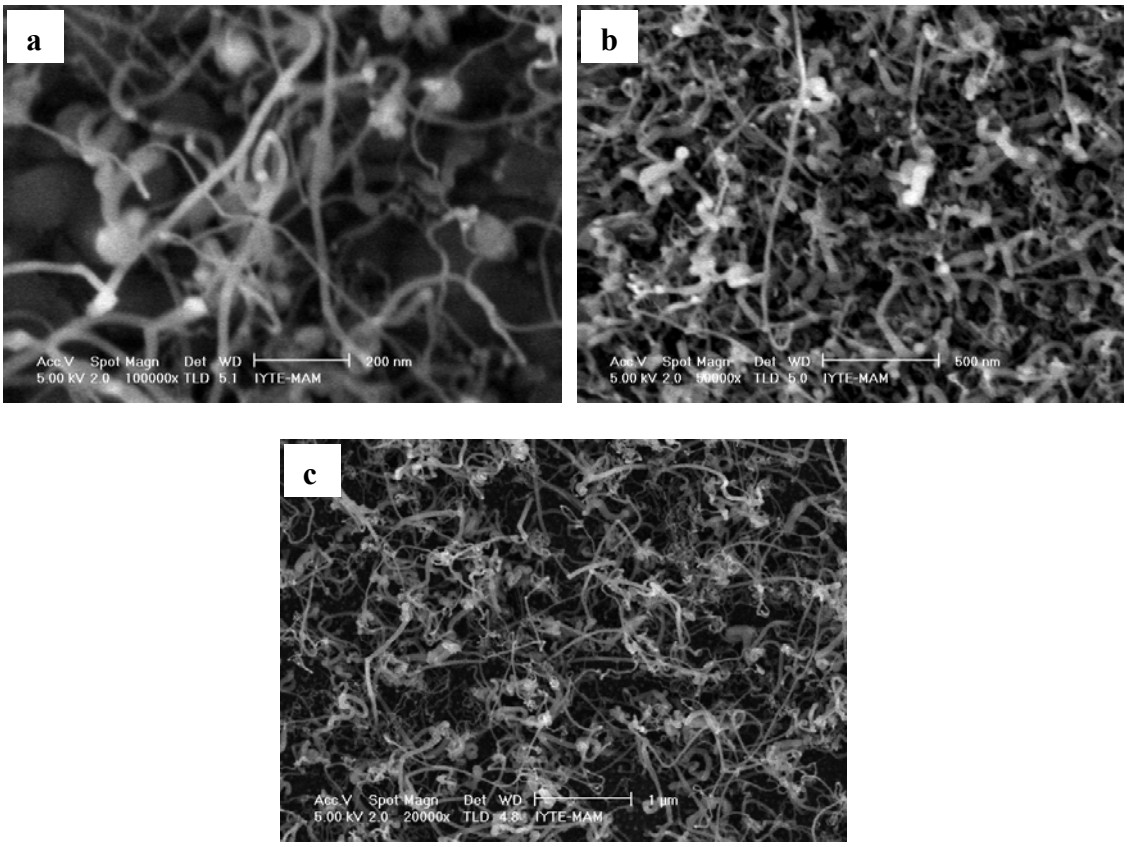

Figure 5.5. SEM micrographs of as- grown CNTs on, a) Fe58/SiO_2/Si at 950°C, b) Fe59/SiO_2/Si at 975°C, c) Fe60/SiO_2/Si at 1000°C

Table 5.2. Comparison of diameters of CNTs grown at different temperatures

Sample Name	Temperature (°C)	CNT Average Diameter (nm)
FeSiO7CNT55	900	20.01
FeSiO7CNT57	925	14.43
FeSiO7CNT58	950	13.86
FeSiO7CNT59	975	18.12
FeSiO7CNT60	1000	38.83

5.1.1.3. CNT Growth on $Co/SiO_2/Si$ Samples

CNT growth was also performed on Co deposited SiO2/Si substrates. In the first place, Co-catalyst nanoparticles were formed on SiO_2/Si thin films at 825°C. The related images are depicted in Figure 5.6.a and Figure 5.6.b with 100000X 50000X magnifications, respectively. It is clearly seen from the images that the catalyst nanoparticles were distributed nearly uniformly on the whole sample surface.

When the catalyst thin films were heated up and etched away by hydrogen gas, the catalyst films were converted to the nanoparticles. Study of SEM images of the CNTs grown on $Co/SiO_2/Si$ thin films at 825°C revealed that no CNT formation was occurred even though methane gas was sent at this temperature. In fact, in our efforts with other Co thin films, not presented here, resulted with no CNT growth at temperatures at and lower than 825 °C. It was observed that nearly uniform formation of Co nanoparticles was achieved with average diameter of about 25 nm.

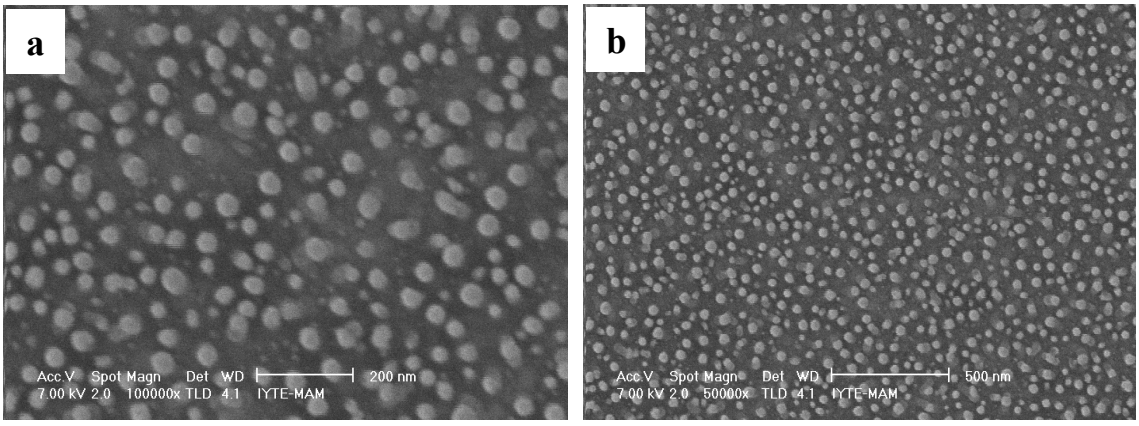

Figure 5.6. SEM micrographs of Co nanoparticles grown on $Co26/SiO_2/Si$ at 825°C, a) magnification: 100000X, b) magnification: 50000X

Hence, the temperature was increased to 850°C, of which result is seen in Figure 5.7.a, depicting that CNT formation was rather bulky and short; the average diameters of CNTs were measured at around 20.4 nm. Furthermore, the temperature was increased to 875°C; the related image is shown in Figure 5.7.b. It was observed that the as-grown CNTs were not well aligned but had the shape of spaghetti with woven each other. And

it is clearly seen from the Figure 5.7.a and Figure 5.7.b that the CNTs were grown with the tip-growth mechanism, since the catalyst nanoparticles were seen at the tip of the CNTs.

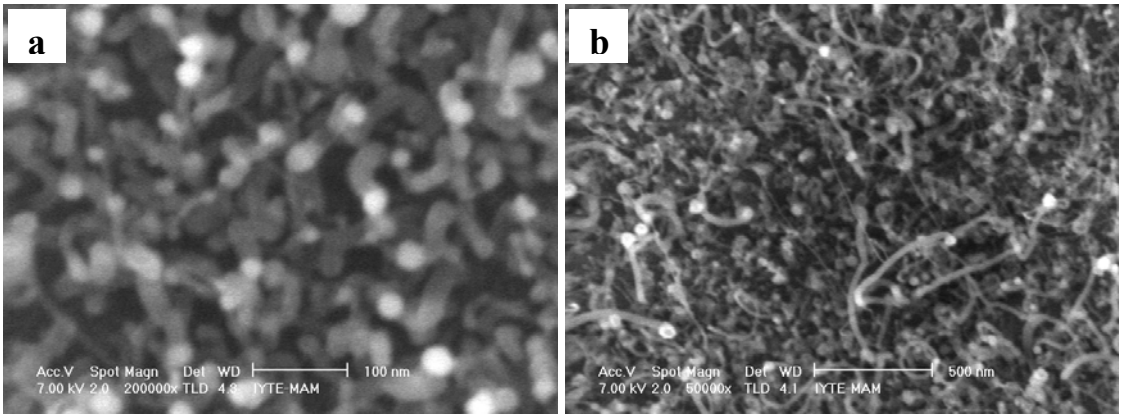

Figure 5.7. SEM micrographs of as-grown CNTs produced onto, a) Co32/SiO_2/Si at 850°C, b) Co33/SiO_2/Si at 875°C

Then, the temperature was increased from 875°C to 900°C; the related SEM images are seen in Figure 5.8.a. and Figure 5.8.b, with 100000 and 50000 magnifications, respectively. From the SEM pictures, the average diameters of CNTs were measured at around ~14.2 nm. The average diameters of as-grown CNTs were decreased with increasing the temperature. From the Figure 5.8, it is seen that the CNTs were grown according to tip-growth mechanism.

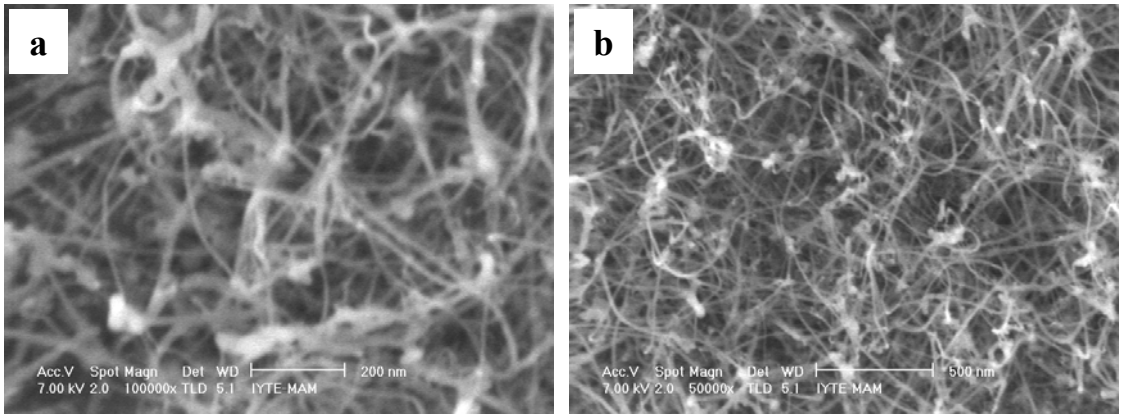

Figure 5.8. SEM micrographs of as-grown CNTs produced onto Co37/SiO_2/Si at 900°C, a) magnification: 100000X, b) magnification: 50000X

The growth temperature was increased from 900°C to 925°C; the related SEM picture is seen in Figure 5.9.a. The average diameters of the CNTs were measured approximately 10.5 nm. When the growth temperature was increased from 925°C to 950°C, of which the result is depicted in Figure 5.9.b, that thinner and longer CNTs were grown with compared to those grown at 925°C and the temperature below 925°C. The average diameters of as-grown CNTs were measured approximately ~13.15 nm; the CNTs were grown with tip-growth mechanism. When the temperature was increased to 975°C, the average diameters of CNTs were measured at around ~18.66 nm. The results were very similar to those obtained for Fe catalyzed CNTs. It was observed that after a critical point, the diameters of CNTs were increasing with increasing the temperature, because of the reasons explained for Fe catalyzed CNTs; after a critical point the surface tension of the catalyst particle was increased, and the dissolution of carbon started again. Then the thickening of the nanotubes occurred layer by layer (Ruemmeli, et al. 2005).

Table 5.3 summarizes the comparison of the average diameter of as-grown CNTs at different temperatures. The results demonstrated how temperature significantly affected the growth of CNTs along with their diameters and lengths.

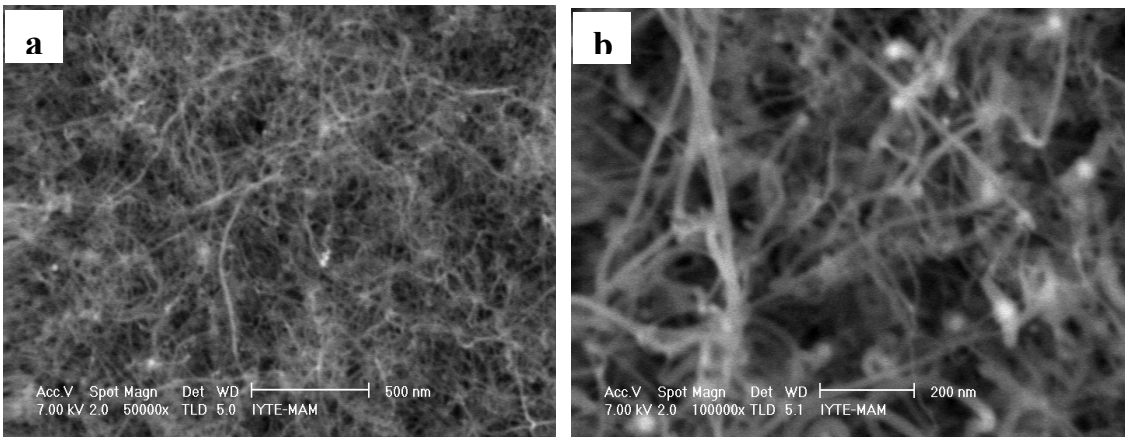

Figure 5.9. SEM micrographs of as-grown CNTs produced onto, a) Co38/SiO_2/Si at 925°C, b) Co39/SiO_2/Si at 950°C

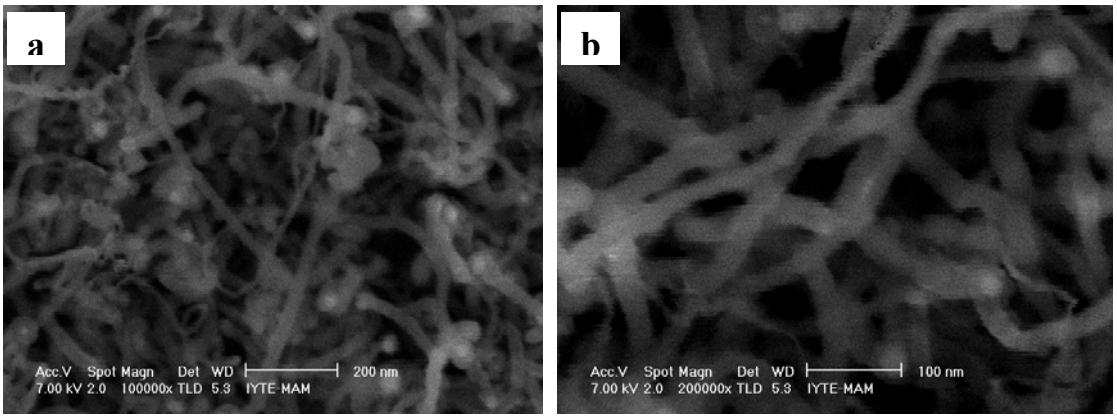

Figure 5.10. SEM micrographs of as-grown CNTs produced at 975°C onto Co49/SiO_2/Si, a) magnification: 100000X, b) magnification: 200000X

Table 5.3. Comparison of diameters of CNTs grown at different temperatures

Sample	Temperature (°C)	Average Diameter (nm)
CoSiO5CNT32	850	20.4
CoSiO5CNT33	875	15.4
CoSiO5CNT37	900	14.2
CoSiO5CNT38	925	10.5
CoSiO5CNT39	950	13.15
CoSiO5CNT49	975	18.66

5.1.2. Catalyst Thickness Effect on the CNT Growth

In this section, Ni catalyst films with three different thicknesses; ~0.7 nm thick named NiSiO1, ~1.4 nm thick named NiSiO2, ~6 nm thick named NiSiO3; were utilized. The growth process was applied for these three catalysts at the same time and at the same temperature; all the parameters were kept constant except the thickness of the catalyst layers in order to observe catalyst layer thickness effect on the CNT growth.

And the CNT growth was performed at the same time for those three Ni catalyst thin films at 900°C. The as-grown CNTs were depicted in Figure 5.11, Figure 5.12, and Figure 5.13 for 0.7 nm, 1.4 nm, and 6 nm thick nickel catalyst films named as NiSiO1CNT78, NiSiO2CNT79, and NiSiO3CNT80, respectively.

It is clearly seen from the images that the CNTs were very well grown on the thinnest (0.7 nm) catalyst layer. Figure 5.11 shows the as-grown CNTs with different magnifications. The average diameters of as-grown CNTs were measured at around 14.42 nm. While the average diameter of the CNTs grown on 1.4 nm thick nickel film was measured approximately 20.74 nm, the related images are seen in Figure 5.12. While there were not so many CNTs on the thickest nickel film which was 6 nm, the related image is depicted in Figure 5.13.

It was investigated that the Ni nanoparticles were grown very small in size on the thinnest film (0.7 nm), whereas very big in size on the thickest film (6 nm). The catalyst nanoparticles were formed very small in size on the thinnest films. When the catalyst nanoparticles were formed very small in size, the carbon atoms would reach the nucleation sites in a short time since the diffusion lengths of the carbon atoms were decreased, and this would result in an increasing in growth rate of CNTs.

On the other hand, when the film thickness was increased, the catalyst nanoparticles would be formed very big in size with compared to those grown on thinner catalyst layers. When the catalyst nanoparticles were very big in size, the carbon atoms would diffuse the nucleation sites in a long time, owing to the fact that the diffusion path of the carbon atoms was increased, which resulted in decreasing the growth rate of CNTS.

The temperature was also increased from 900°C to 950°C, so as to examine the temperature effect on Ni catalyst films with three different thicknesses. The results are depicted in Figure 5.14.a, b, and c for 0.7 nm, 1.4 nm, and 6 nm thick Ni catalyst films, respectively. It was observed that when the temperature was increased, the average diameter of CNTs was decreased and the length was also increased, of which the results were in agreement with those CNTs grown on Fe and Co catalyst thin films. When the temperature was increased from 900°C to 950°C, the diameters were decreased from ~14.42 nm to ~9.35 nm for NiSiO1 films, and in a similar manner, it was decreased from ~20.74 nm to ~17.42 nm for NiSiO2 catalyst film. The results are given in Table 5.4.

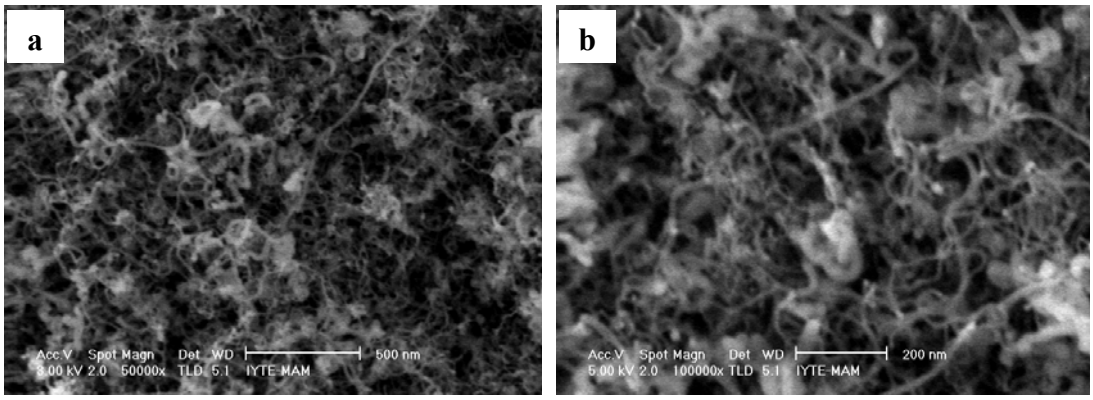

Figure 5.11. SEM micrographs of as-grown CNTs on NiSiO1CNT78 at 900°C, a) magnification: 50000X, b) magnification: 100000X, thickness: ~0.7 nm

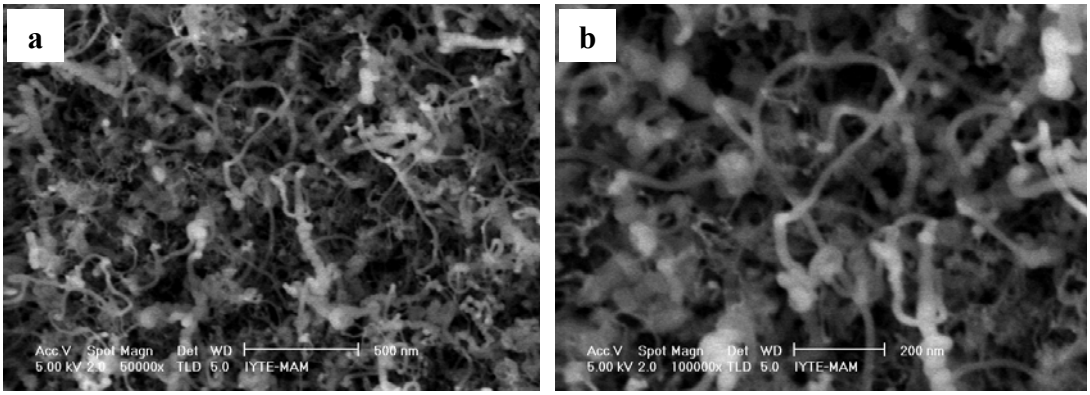

Figure 5.12. SEM micrographs of as- grown CNT on NiSiO2CNT79 at 900°C, a) magnification: 50000X, b) magnification: 100000X, thickness: ~1.4 nm

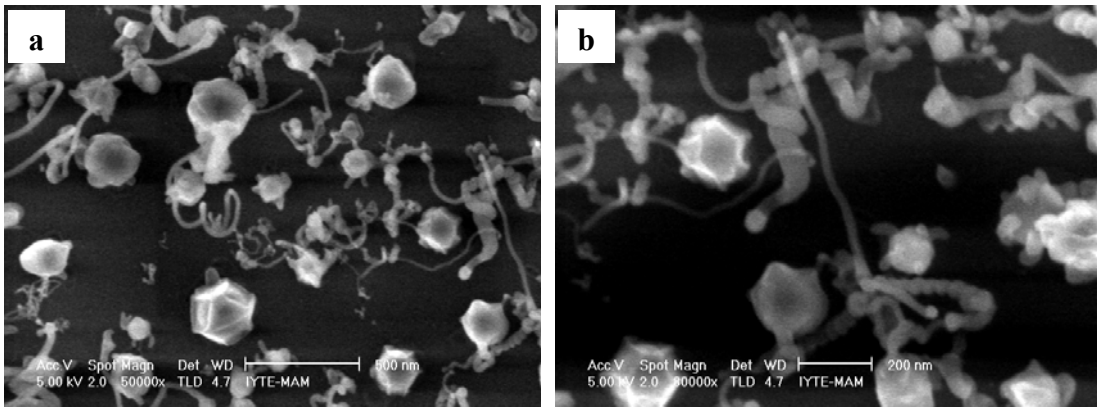

Figure 5.13. SEM micrographs of as-grown CNT on NiSiO3CNT80 at 900°C, a) magnification: 50000X, b) magnification: 100000X, thickness: ~6 nm

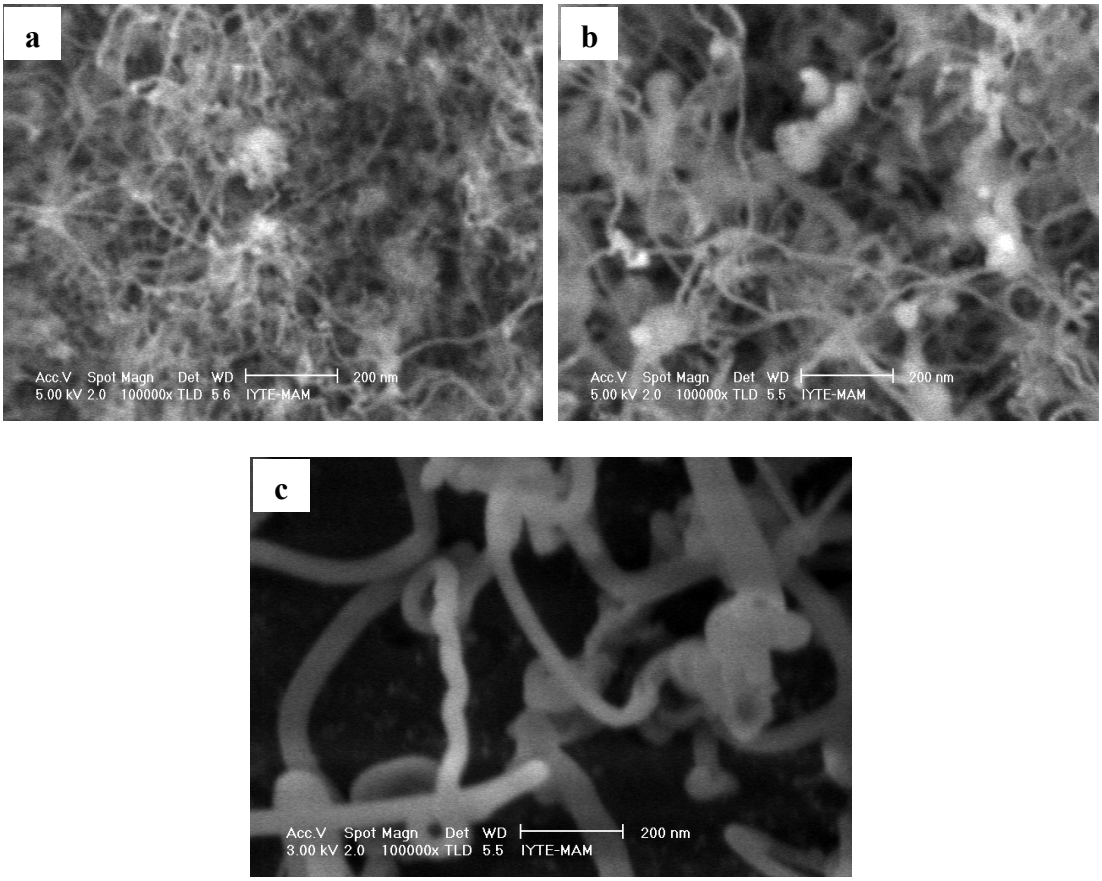

Figure 5.14. SEM micrographs of as-grown CNTs at 950°C on Ni catalyst thin films with three different thicknesses, a) NiSiO1CNT81: ~0.7 nm, b) NiSiO2CNT82: ~1.4 nm, c) NiSiO3CNT83: ~6 nm

Table 5.4. Comparison of diameters of CNTs grown on Ni catalyst thin films with different thicknesses and temperatures

Sample Name	**Catalyst Thickness (nm)**	**Temperature (□C)**	**CNT Average Diameter (nm)**
NiSiO1CNT78	~0.7 nm	900	~14.42
NiSiO2CNT79	~1.4 nm	900	~20.74
NiSiO1CNT81	~0.7 nm	950	~9.35
NiSiO2CNT82	~1.4 nm	950	~17.42

5.2. AFM RESULTS

The roughness values of two Ni catalyst thin films, NiSiO1 (~0.7 nm/1 min) and NiSiO2 (~1.4 nm/2 min), deposited on SiO2/Si substrates onto which no CNT growth was performed were also measured by utilizing the AFM. The related AFM images are depicted in Figure 5.15.a and Figure 5.15.b. The rms surface roughness values were measured as 0.205 nm, and 0.305 nm for NiSiO1 (~0.7 nm/1 min) and NiSiO2 (~1.4 nm/2 min), respectively. The roughness values are given in Table 5.5.

On one hand, these values were very satisfying since from the view of thin film technology, it showed that those catalyst thin films were deposited uniformly and continuously. If rms surface roughness is smaller than the catalyst film thickness it means that the thin film is deposited uniformly. On the other hand, the increase in rms surface roughness is associated with an increase in some irregularities in the film; which results in an increase the size of the catalyst nanoparticles.

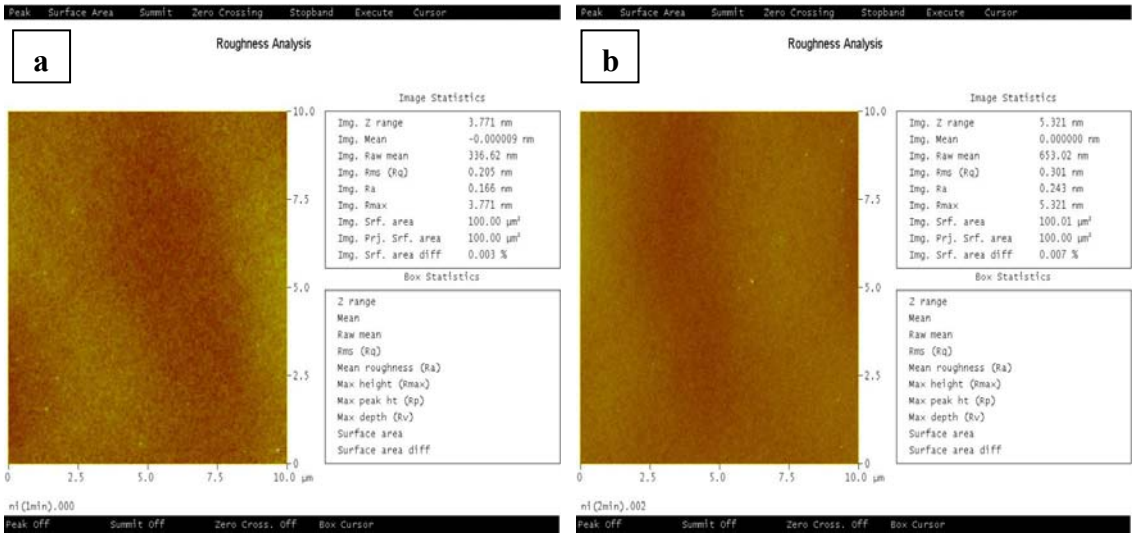

Figure 5.15. Roughness analyses of, a) NiSiO1 (~0.7 nm), b) NiSiO2 (~1.4 nm)

Table 5.5. Roughness values of Ni catalyst thin films

Sample Name	Catalyst Thickness (nm)	Rms Surface Roughness (nm)
NiSiO1	~0.7 nm	0.205
NiSiO2	~1.5 nm	0.301

5.3. XRD Results

The XRD measurement (θ-2θ Scan) was carried out using CuK_α radiation with λ= 1.54 Å so as to characterize the CNT structures. Since CNTs are composed of many graphitic planes made of carbon atoms, the XRD characterization gives good information about the CNT structure. The graphs exhibit characteristic peaks of CNTs.

From the literature, the peak seen at around 26.2° indexed by (002) illustrates of being CNTs. Also, the peak at around 77.7° (or 78°) indexed by (110) also corresponds to CNTs (Park, et al. 2002). The peak at around 43.95° (or 44°) indicates CNT (101) structure (Treffer, et al. 1997), while the peak at 38° corresponds to SiC (101) and also SiC (220) is seen at around 61° (Treffer, et al. 1997, Bhuyan, et al. 2007). Substrates peaks are Si (002) planes, 32.88°, Si (004) plane, 69.08°.

Figure 5.16 shows a typical XRD pattern of as-grown CNTs for CoSiO5CNT32 taken with θ–2θ scan mode. It is seen from the picture that, the peak seen at 26° is ascribable to CNT (002) planes, while the peaks seen nearly at 44° refers to CNT (101), whereas the CNT (110) peak is seen at around 78°. There is also one broad peak seen at around 69.08° is coming from the Si substrate, while the other sharp and thin peak around 38° is considered to be SiC (101) plane (Bhuyan, et al. 2007). It is sensible to see SiC (101) peak due to the fact that it is desired to see some carbide peaks since they have an important role in the growth of CNTs.

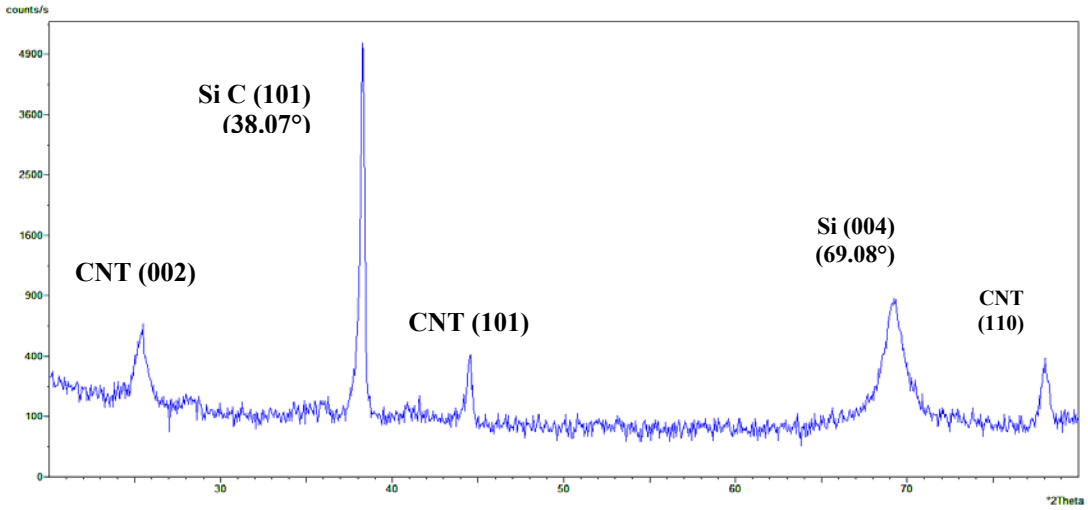

Figure 5.16. XRD pattern of as-grown CNTs onto CoSiO5CNT32

Figure 5.17 is the XRD pattern of the as-grown CNTs for CoSiO5CNT38. The peak at $2\theta = 26.24°$ is attributed to the diffractions of (002) planes of the hexagonal graphite structure, and 32° and 69° contribute to substrates peaks. The peaks seen at nearly 35°, 38, and 61° refer to SiC peaks from the planes of (111), (101), and (220), respectively. Peaks seen at around 44° and 78° contribute to CNT (101) and CNT (110), respectively.

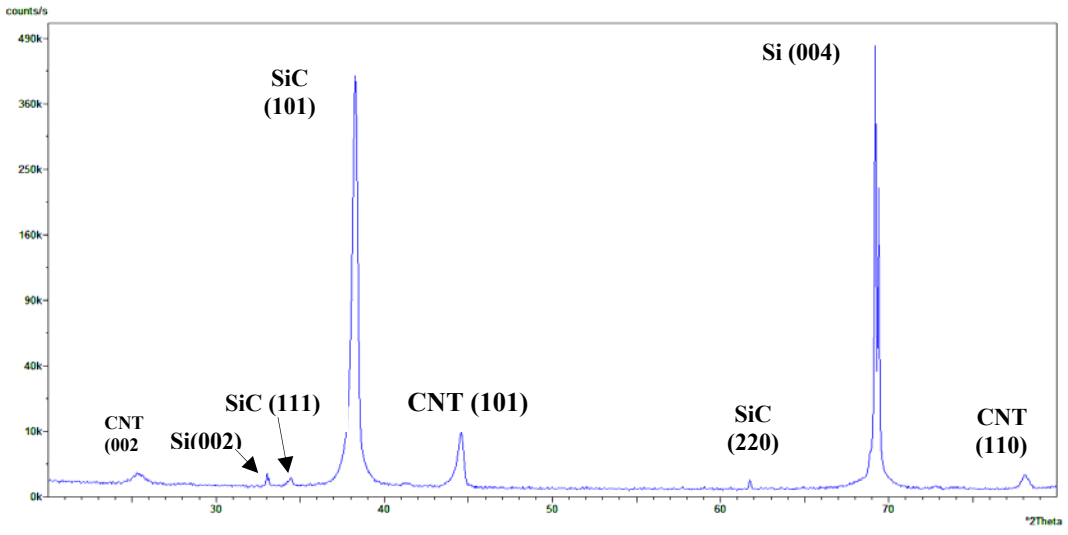

Figure 5.17. XRD pattern of as-grown CNTs onto CoSiO5CNT38

Figure 5.18 is the XRD pattern of the as-grown CNTs for CoSiO5CNT38. The peaks at $2\theta = 26.24°$, 44° and 78° contribute to CNT (002), CNT (101), and CNT (110), respectively; and 69° attributes to Si (004); 38, and 61° refer to SiC peaks from the planes of (101), and (220), respectively.

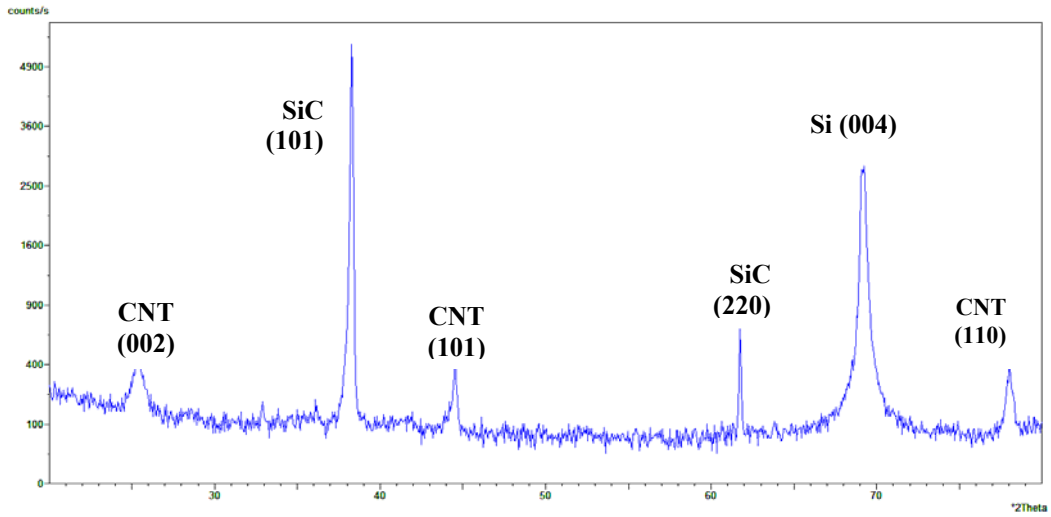

Figure 5.18. XRD pattern of as-grown CNTs onto CoSiO5CNT49

5.4. Raman Spectroscopy Results

Micro-Raman Spectroscopy with He-Ne laser with the excitation wavelength of 632.8 nm (633nm) was utilized for some the samples so as to observe the quality of CNTs as well as their types, whether they were semiconductor or metallic.

Figure 5.19 depicts the Raman spectra of FeSiO7CNT58. Figure 5.19 shows that the graph definitely proved the presence of SWNTs. Figure 5.19 is the Raman signature of semiconducting SWNTs with very few defects (low D band intensity). These CNTs were of a very high structural purity because of the fact that there was very small intensity of D-band around 1300 cm^{-1}, and it is also seen from the image that the G-band at around 1594 cm^{-1} was very narrow having also a shoulder at around 1558 cm^{-1} meaning that the as-grown SWNTs were semiconducting CNTs.

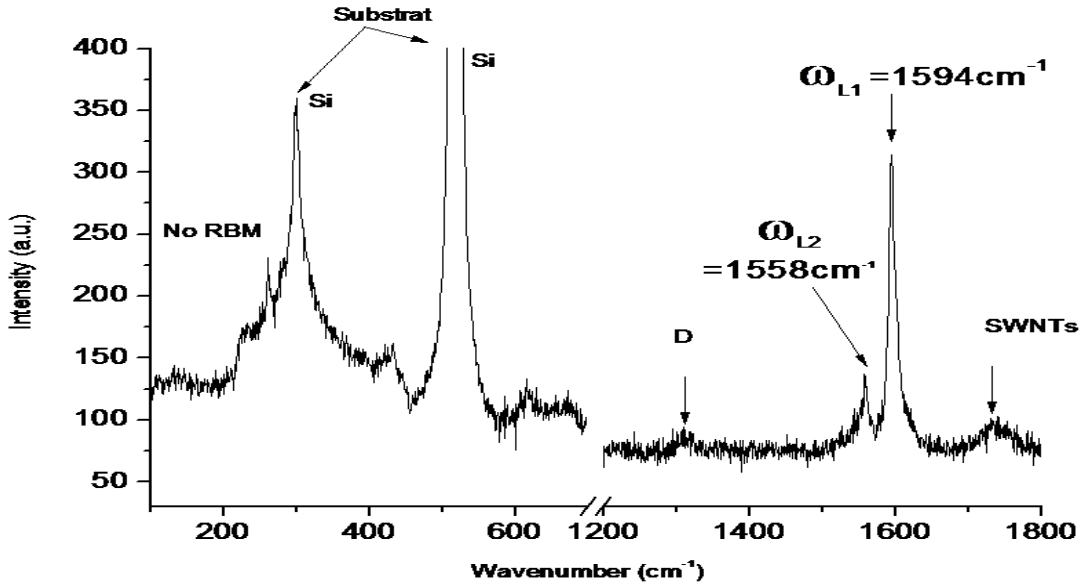

Figure 5.19. Raman spectra of as-grown CNTs on FeSiO7CNT58 thin film

Figure 5.20 illustrates the Raman spectra of as-grown CNTs on FeSiO7CNT59 catalyst thin film. He-Ne Laser 633 nm on a $2\mu^2$ area was taken from three different points on Fe59SiO7 area seen with the colors of blue, red, and black. Clearly seen from the Figure 5.20 that the spectra had mainly four Raman bands two of which were coming from the substrates while the other bands were seen at nearly ~1335 cm^{-1} (D band), and ~1580 cm^{-1} (G band). The G band indicates original graphite features but the D band displays the disorder features of graphitic sheets meaning that D mode is a sign for the defective graphitic structures.

The comparison of the ratios of these two peaks gives a measure of quality of the bulk samples. Depicted in Figure 5.20, there were disordered MWCNTs signal coming from the sample. And also, the intensity of D line was bigger than the G-line intensity which indicated that there were defects in the structure of CNTs and those CNTs showed metallic behavior.

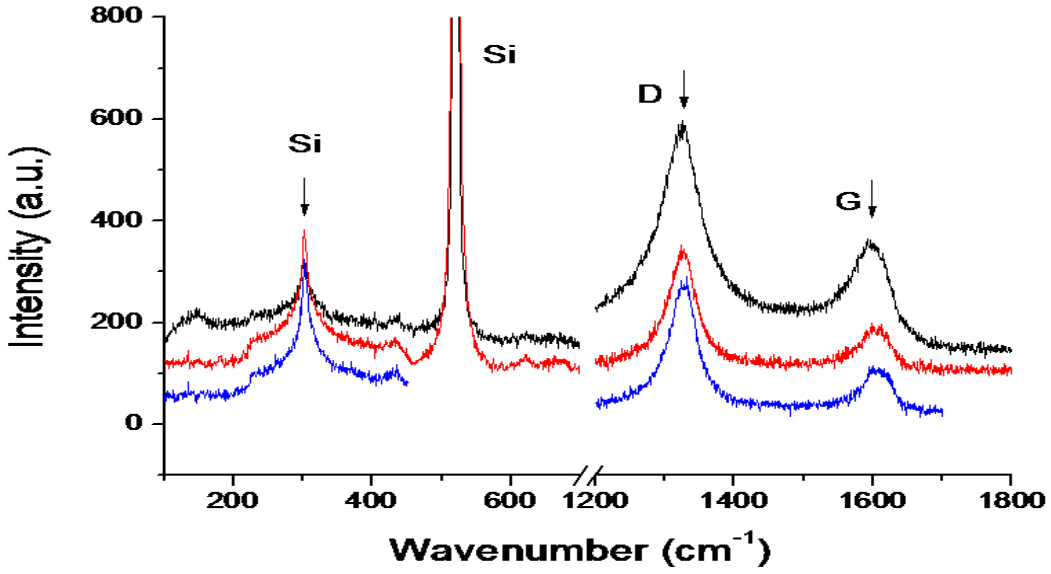

Figure 5.20. Raman spectra of as-grown CNTs on FeSiO7CNT59 thin film

Figure 5.21 is the Raman spectra of as-grown CNTs on NiSiO1CNT81 catalyst thin film. Depicted in Figure 5.21 that the longitudinal Raman bands of semiconducting SWNTs peaks were 1597 and 1567 cm^{-1}, which were very narrow line (nearly 9 cm^{-1}), meaning that the as-grown CNTs were really well crystallized. There was a little trace of disordered carbon phases around 1320 cm^{-1}. This graph definitely proved that the as-grown CNTs were semiconducting SWNTs with very low defects.

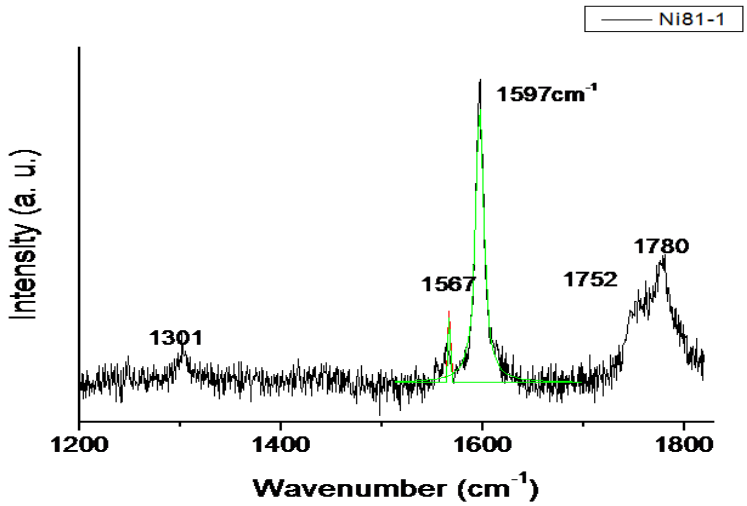

Figure 5.21. Raman spectra of as-grown CNTs on NiSiO1CNT81 thin film

Figure 5.22 illustrates the Raman spectra of as-grown CNTs on CoSiO5CNT39 catalyst thin film. If there is only the band at 1594 cm^{-1}, it corresponds to very well crystallized MWNTs. Clearly seen from the spectra, there was no trace of signal around 1300 cm^{-1} meaning that there was no trace of disordered carbon phases.

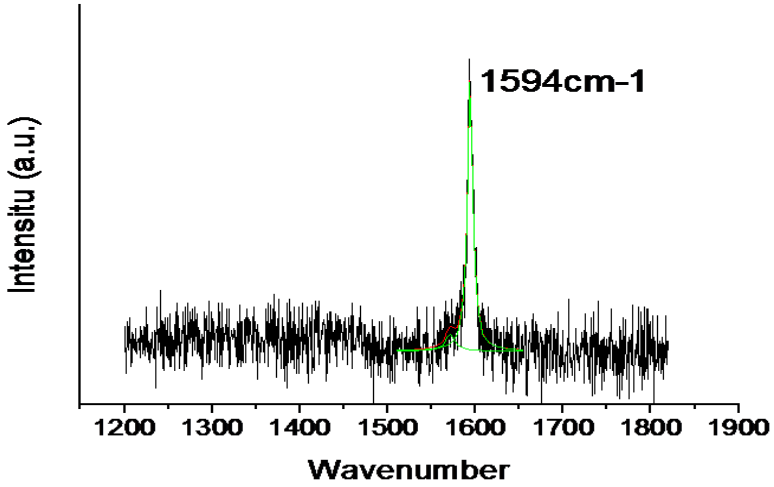

Figure 5.22. Raman spectra of as-grown CNTs on CoSiO5CNT39 thin film

CHAPTER 6

CONCLUSION

In this thesis work, the parameters were optimized and some parameters affecting the growth of CNTs were examined. In the first place, the CNTs growth was performed on directly bare Si substrates at four different temperatures, 800, 850, 900, and 950°C. It was observed that there was no CNT growth on Si but mostly amorphous carbon, due to the fact that the solubility of C atoms in Si nanoparticles was too low at the temperatures; 800, 850, 900, and 950°C and it required very high temperatures.

Furthermore, the temperature effect was systematically studied by utilizing Co and Fe thin films. It was obtained that the average diameter of as-grown CNTs were decreased with increasing the temperature up to a critical point, and then that the average diameter of those CNTs' was increased after this critical point. The similar results were observed for Co and Fe catalyst thin films. The reason of this thickening of the CNTs was explained by the means of surface tension and the size of the catalyst nanoparticle.

Moreover, the thickness effect of the catalyst thin film layer on the CNT growth was also examined by utilizing Ni thin films with three different thicknesses as 0.7, 1.4, and 6 nm, keeping all the other parameters constant. When the thickness of the catalyst layer was increased, the average diameters of the catalyst nanoparticles were increased which leaded an increase in the carbon atoms diffusion length, and so for low growth rate. So it was reached the conclusion that the thinnest catalyst thin film leaded CNTs to be very small in size, on the contrary the thickest thin film caused CNTs to be bigger in size.

The experiments were performed at both 900 and 950°C by utilizing the Ni catalyst thin films with three different thicknesses by comparing the average diameter of as-grown CNTs by increasing the temperature from 900°C to 950°C. When the temperature was increased from 900°C to 950°C, it was observed that the average diameters of CNTs were decreased, which was very compatible with the results obtained for the temperature effect on the growth of CNTs by utilizing Fe and Co thin films.

The Ni catalyst thin films with 0.7 nm and 1.4 nm thickness were utilized for the measurement rms surface roughness values. Obtained from AFM results that the rms surface roughness value was increased with increasing the thickness, meaning that the average diameter of catalyst nanoparticles grown on 0.7 nm thin film was smaller in size than the catalyst nanoparticles produced on 1.4 nm thin film.

Some of the as-grown CNTs were also examined by micro-Raman spectroscopy to have an accurate idea about not only the type of the CNTs but also the quality of them. It was observed that the as-grown CNTs produced on Ni and Fe catalyst thin films were SWNTs showing semiconducting behavior with very low defect, but MWNTs were observed on Co deposited catalyst thin films. The Raman spectroscopy results were in agreement with SEM results.

Moreover, XRD was utilized in order to have the structural information and chemical composition of as-grown CNTs. As expected, CNTs peaks coming from different planes along with SiC peaks and Si substrates peaks were observed.

REFERENCES

Ago, H., K. Murata, M. Yumura, J. Yotani, and S. Uemura. 2003. Ink-jet printing of nanoparticle catalyst for site-selective carbon nanotube growth. *Applied Physics Letters* 82:811-819.

Ago, H., T. Komatsu, S. Ohshima, Y. Kuriki, and M. Yumura. 2000. Dispersion of metal nanoparticles for aligned carbon nanotube arrays. *Applied Physics Letters* 77:79-82.

Alexandrou, I., H. Wang, N. Sano, and G. A. J. Amaratunga. 2004. Structure of carbon onions and nanotubes formed by arc in liquids. *Journal of Chemical Phys*ics 120:1055-1058.

Ando, Y., X. Zhao, T. Sugai, and M. Kumar. 2004. Growing carbon nanotubes. *Materials Today* 1369(7):22-29.

Arthur, J. and A. Cho. 1973. Adsorption and desorption kinetics of Cu and Au on (0001) graphite. *Surface Science* 36:64-660.

Avouris, P. 2002. Carbon nanotube electronics. *Chemical Physics* 28:429-445.

Baker, R.T.K. and P.S. Harris. 1978. *Formation of filamentous carbon in chemistry and physics of carbon 14*. New York: Marcel Dekker.

Baker, R.T.K., M.A. Barber, P.S. Harris, F.S. Feates, and R.J. Waite. 1972. Nucleation and growth of carbon deposits from the nickel catalyzed decomposition of acetylene. *Journal of Catalysis* 26:51-62.

Baughman, R.H., A.A. Zakhidov, and W.A. Heer. 2002. Carbon Nanotubes-the route towards Applications. *Science* 297(5582):787-792.

Bethune, D.S., C.H. Kiang, M.S. Vries, G. Gorman, R. Savoy, J. Vazquez, and R. Beyers. 1993. Cobalt-catalyzed growth of CNTs with single atomic layer walls. *Nature* 363:605-607.

Begtrup, G. E., K.G. Ray, B.M. Kessler, T.D. Yuzvinsky, H. Garcia, and A. Zettl. 2007. Extreme thermal stability of carbon nanotubes. *Physica Status Solidi (b)* 244(11):3960-3963.

Bhuyan H, M. Favre, E. Valderrama, G. Avaria , H. Chuaqui, I. Mitchell, E. Wyndham, R. Saavedra, and M. Paulraj. 2007. Formation of hexagonal silicon carbide by high energy ion beam irradiation on Si(100) substrate. *Journal of Physics D: Applied Physics* 40:127-131.

Cheng, H.M., S.F. Li, G. Pan, H.Y. Pan, L.L. He, and X. Sun. 1998. Large-scale and low-cost synthesis of single-walled carbon nanotubes by the catalytic pyrolysis of hydrocarbons. *Applied Physics Letters* 72:3282-3284.

Cheung, C.L., A. Kurtz, H. Park, and C.M. Lieber. 2002. Diameter-controlled synthesis of carbon nanotubes. *Journal of Physical Chemistry B* 106:2429-2433.

Cho, Y.S., G.S. Choi, S.Y. Hong, and D. Kim. 2002. Carbon nanotube synthesis using a magnetic fluid via thermal chemical vapor deposition. *Journal of Crystal Growth* 243:224-229.

Choi, Y.C., Y.M. Shin, Y.H. Lee, B.S. Lee, G.S. Park, and W.B. Choi. 2000. Controlling the diameter, growth rate, and density of vertically aligned carbon nanotubes synthesized by microwave plasma-enhanced chemical vapor deposition. *Applied Physics Letters* 76:2367-2372.

Colbert D.T, M. Zhang, S.M. McClure, P. Nikolaev, Z. Chen, , J.H. Hafner, D.W. Owens, P.G. Kotula, C.B. Carter, J.H. Weaver, A.G. Rinzler, and R. E. Smalley. 1994. Growth and sintering of fullerene nanotubes. *Science* 266:1218-1222.

Colomer, J.F., J.F. Bister, I. Willems, Z. Konya, A. Fonseca, and G. V. Tendeloo. 1999. Synthesis of single-wall carbon nanotubes by catalytic decomposition of hydrocarbons. *Chemical Commun*ications 14:1343-1344.

Colomer, C., S. Stephan, G. Lefrant, V. Tendeloo, I. Willems, and Z. Kónya. 2000. Large-scale synthesis of single-wall carbon nanotubes by catalytic chemical vapor deposition (CCVD) method. *Chemical Physics Letters* 317:83-89.

Cui, H., O. Zhou, and B.R. Stoner. 2000. Deposition of aligned bamboo-like carbon nanotubes via microwave plasma enhanced chemical vapor deposition. *Journal of Applied Physics* 88(10):6072-6077.

Dai H. 2002. Carbon nanotubes: opportunities and challenges. *Surface Science* 500:218-241.

Deck, C.P. and K. Vecchio. 2006. Prediction of Carbon nanotube growth success by the analysis of carbon-catalyst binary phase diagrams. *Carbon* 44:267-275.

Dresselhaus, Mildred S., Gene Dresselhaus, and Phaedon Avouris, eds. 2001. *Carbon nanotubes: synthesis, structure, properties, and applications*. Berlin: Springer Publishers.

Dresselhaus, M.S., G. Dresselhaus, A. Jorio, A.G.S. Filho, and R. Saito. 2002. Raman Spectroscopy on isolated single wall carbon nanotubes. *Carbon* 40:2043-2061.

Dresselhaus, M.S., Y. M. Lin, O. Rabin, A. Jorio, A.G. Souza, M.A. Pimenta, R. Saito, G.G. Samsonidze, and G. Dresselhaus. 2003. Nanowires and nanotubes. *Materials Science and Engineering C* 23(1-2):129-140.

Duesberg, G.S., A.P. Graham, M. Liebau, R. Seidel, E. Unger, F. Kreupl, and W. Hoenlein. 2003. Growth of isolated carbon nanotubes with lithographically defined diameter and location. *Nano Lett*ers 3(2):257-259.

Dupuis, A.C. 2005. The catalyst in the CCVD of carbon nanotubes: a review. *Progress in Materials Science* 50(8):929-961.

Ebbesen, T.W. 1994. Carbon nanotube. *Annual Review Matterials* 24:235-264.

Eklund, C., M. Holden, and A. Jishi. 1995. Vibrational modes of carbon nanotubes, spectroscopy and Theory. *Carbon* 33(7):959-972.

Ermakova, M.A., D.Y. Ermakov, A.L. Chuvilin, and G.G. Kuvshinov. 2001. Decomposition of methane over iron catalysts at the range of moderate temperatures: the influence of structure of the catalytic systems and the reaction conditions on the yield of carbon and morphology of carbon filaments. *Journal of Catalysis* 201:183-197.

Feldman, Leonard C. and James W. Mayer. 1986. *Fundamentals of surface and thin film analysis*. New Jersey: PTR Prentice-Hall, Inc.

Fonseca, A., K. Hernadi, J.B. Nagy, D. Bernaerts, and A.A. Lucas. 1996. Optimization of catalytic production and purification of buckytubes. *Journal of Molecular Catalysis A: Chemical* 107:159-168.

Guo, T., P. Nikolaev, A. Thess, D.T. Colbert, and R.E. Smalley. 1995. Catalytic growth of single-walled nanotubes by laser vaporization. *Chemical Physics Letters* 243:49-54.

Guo, T, P. Nikolaev, A.G. Rinzler, D. Tomanek, D. T. Colbert, and R.E, Smalley. 1995. Self-assembly of tubular fullerenes. *Journal of Physical Chemistry* 99(27): 10694-10697.

Guan, L., K. Suenaga, and S. Iijima. 2008. Smallest carbon nanotube assigned with atomic resolution accuracy. *Nano Letters* 8(2):459-462.

Hansen, Max and Kurt Anderko. 1958. *Constitution of binary alloys*. New York: McGraw-Hill.

Harris, P. J. F. 2007. Solid state growth mechanisms for carbon nanotubes. *Carbon* 45:229-239.

Hayashi, T., Y.A. Kim, T. Matoba, M. Esaka, K. Nishimura, T. Tsukada, M. Endo, and M.S. Dresselhaus. 2003. Smallest freestanding single-walled carbon nanotube. *Nano Letters* 3(7):887-889.

Hernadi, K., A. Fonseca, J.B. Nagy, D. Bernaerts, A. Fudala, and A.A. Lucas. 1996. Catalytic synthesis of carbon nanotubes using zeolite support. *Zeolites* 17:416-423.

Heer, W.A. and D. Ugrate. 1993. Carbon onions produced by heat treatment of carbon soot and their relation to the 217.5 nm interstellar absorption feature. *Chemical Physics Letters* 207:480-486.

Hone, J., W. Whitney, C. Piskoti, and A. Zettle. 1999. Thermal conductivity of single-walled carbon nanotubes. *Physical Review B* 59(4):2514-2516.

Hongo, H., M. Yudasaka, T. Ichihashi, F. Nihey, and S. Iijima. 2002. Chemical vapor deposition of single-wall carbon nanotubes on iron-fill-coated sapphire substrates. *Chemical Physics Letters* 361:349-354.

Hsu, C.M., C.H. Lin, H.L. Chang, and C.T. Kuo. 2002. Growth of the large area horizontally-aligned carbon nanotubes by ECR-CVD. *Thin Solid Films* 420:225-229.

Huang, Z.P., J.W. Xu, Z.F. Ren, J.H. Wang, M.P. Siegal, and P.N. Provencio.1998. Growth of highly oriented carbon nanotubes by plasma-enhanced hot filament chemical vapor deposition. *Applied Physics Letters* 73:3845-3846.

Iijima, S. 1991. Helical microtubules of graphitic carbon. *Nature* 354:56-58.

Iijima, S. and T. Ichihashi. 1993. Single-shell carbon nanotubes of 1 nm diameter. *Nature* 363:603-605.

Ivanov, V., J. B. Nagy, P. Lambin, A. Lucas, X.F. Zhang, and D. Bernaerts. 1994. The study of carbon nanotubules produced by catalytic method. *Chemical Physics Letters* 223:329-335.

Ivchenko, E.L. and B. Spivak. 2002. Chirality effects in carbon nanotubes. *Physical Review B* 66(15):155404-155413.

Jiao, J. and S. Seraphin. 2000. Single-walled tubes and encapsulated nanoparticles: comparison of structural properties of carbon nanoclusters prepared by three different methods. *Journal of Physics and Chemistry of Solids* 61:1055-1067.

Journet, C. and P. Bernier. 1998. Production of carbon nanotubes. *Applied Physics A* 67:1-9.

Kajiura, H., S. Tsutsui, K. Kadono, M. Kakuta, M. Ata, and Y. Murakami. 2003. Hydrogen storage capacity of commercially available carbon materials at room temperature. *Applied Physics Letters* 82(7):1105-1110.

Kiang, C. H. 2000. Carbon rings and cages in the growth of single-walled carbon nanotubes. *Journal of Chemical Physics* 113(11):4763-4767.

Klinke,C., J.-M. Bonard, and K. Kern. 2001. Comparative study of the catalytic growth of patterned carbon nanotube films. *Surface Science* 492:195-201.

Kong, J., A.M. Cassell, and H. Dai. 1998. Chemical vapor deposition of methane for single-walled carbon nanotubes. *Chemical Physics Letters* 292(4):567-574.

Kroto, H.W., J.R. Heath, S.C. O'Brien, R.F. Curl, R.E. Smalley. 1985. C60: buckminsterfullerene. *Nature* 318:162-163.

Kukovecz, A., Z. Kónya, N. Nagaraju, I. Willems, A. Tamási, A. Fonseca, J.B. Nagy, I. Kiricsi. 2000. Catalytic synthesis of carbon nanotubes over Co, Fe and Ni containing conventional and sol–gel silica–aluminas. *Physical Chemistry Chemical Physics* 2:3071-3076.

Kukovitsky, E.F., S.G. L'vov, N.A. Sainov, V.A. Shustov, and L.A. Chernozatonskii. 2002. Correlation between metal catalyst particle size and carbon nanotube growth. *Chemical Physics Lett*ers 355:497-503.

Laurent, C., E. Flahaut, A. Peigney, and A. Rousset. 1998. Metal nanoparticles for the catalytic synthesis of carbon nanotubes. *New Journal of Chemistry* 1229-1237.

Lee, C. J., J. Park, and J.A. Yu. 2002. Catalyst effect on carbon nanotubes synthesized by thermal chemical vapor deposition. *Chemical Physics Letters* 360:250-255.

Lee C.J., J. Park, Y. Huh, and J.Y. Lee. 2001. Temperature effect on the growth of CNTs using thermal chemical vapor deposition. *Chemical Physics Letters* 343: 33-38.

Li, Y., W. Kim, Y. Zhang, M. Rolandi, D. Wang, and H. Dai. 2001. Growth of single-walled carbon nanotubes from discrete catalytic nanoparticles of various sizes. *Journal of Physical Chemistry B* 105:11424-11431.

Makris, D.T., L. Giorgi, R. Giorgi, N. Lisi, and E. Salernitano. 2005. CNT growth on alumina supported nickel catalyst by TCVD. *Diamond and Related Materials* 14:815-819.

Maultzsch, J., S. Reich, and C. Thomsen. 2002. Raman scattering in carbon nanotubes revisited. *Physical Review B* 65:233402-233406.

Marty, L., V. Bouchiat, A.-M. Bonnot, M. Chaumont, T. Fournier, S. Decossass, and S. Rocha. 2002. Batch processing of nanometer-scale electrical circuitry based on in-situ grown single-walled carbon nanotubes. *Microelectronic Engineering* 61:485-489.

Merkoci, A. 2006. Carbon nanotubes in analytical sciences. *Microchimica Acta* 152:157-174.

Moisala, A., A.G. Nasibulin, and E.I. Kapauppinen. 2003. The role of metal nanoparticles in the catalytic production of single-walled carbon nanotubes. *Journal of Physics: condensed matter* 15:3011-3035.

Monthioux, M. and V. L. Kuznetsov. 2006. Who should be given the credit for the discovery of carbon nanotubes. *Carbon* 44(9):1621-1623.

Nikolaev, P., M. Bronikowski, R. Bradley, F. Rohmund, D. Colbert, K. Smith, and R.E. Smalley. 1999. Gas-phase catalytic growth of single-walled carbon nanotubes from carbon monoxide. *Chemical Physics Letters* 313(1):91-97.

Oberlin A, M. Endo, T. Koyama. 1976. Filamentous growth of carbon through benzene decomposition. *Journal of Crystal Growth* 32:335-349.

O'Connor Daniel. J., Brett A. Sexton, Roger St. C. Smart. 2003. *Surface analysis methods in materials science*. New York: Springer Publishers.

Pan, S.S., Z.W. Xie, B.H. Chang, L.F. Sun, W.Y. Zhou, and G. Wang. 1999. Direct growth of aligned open carbon nanotubes by chemical vapor deposition. *Chemical Physics Letters* 299:97-102.

Park J.B, G.S. Choi, Y.S. Cho, S.Y. Hong, D. Kim, S.Y. Choi, J.H. Lee, K. Cho. 2002. Characterization of Fe-catalyzed carbon nanotubes grown by thermal chemical vapor deposition. *Journal of Crystal Growth* 244:211-217.

Pérez-Cabero, M., I. Rodríguez-Ramos, and A. Guerrero-Ruíz. 2003. Characterization of carbon nanotubes and carbon nanofibers prepared by catalytic decomposition of acetylene in a fluidized bed reactor. *Journal of Catalysis* 215:305-316.

Popov, V. N. 2004. Carbon nanotubes: properties and applications. *Materials Science and Engineering Reports* 43:61-102.

Qingwen, L., Y. Hao, C. Yan, Z. Jin, L. Zhongfan. 2002. A scalable CVD synthesis of high purity single walled carbon nanotubes with porous MgO as support material. *Journal of Materials Chemistry* 12:1179-1183.

Radushkevich LV, V.M. Lukyanovich. 1952. O strukture ugleroda, obrazujucegosja pri termiceskom razlozenii okisi ugleroda na zeleznom kontakte. *Zurn Fisic Chim* 26: 88-95.

Rao, A.M., E. Richter, S. Bandow, B. Chase, P.C. Eklund, K.A. Williams, S. Fang, K.R. Subbaswamy, M. Menon, A. Thess, R.E. Smalley, G. Dresselhaus, and M.S. Dresselhaus. 1997. Diameter-selective raman scattering from vibrational modes in carbon nanotubes. *Science* 275:187-191.

Reich, S., C. Thomsen, and J. Maultzsch. 2004. *Carbon nanotubes: basic concepts and physical properties*. Berlin: Wiley-VCH.

Ren, Z.F., Z.P. Huang, J.W. Xu, J.H. Wang, P. Bush, and M.P. Siegal.1998. Synthesis of large arrays of well-aligned carbon nanotubes on glass. *Science* 282:1105-1107.

Richardson, J. T. 1989. *Principles and catalyst development*. New York: Plenum Press.

Roth, Siegmar and David Carroll. 2004. *One dimensional Metals*. Berlin: Wiley-VCH.

Rotkin, Slava V. and Shekhar Subramoney, eds. 2005. *Applied physics of carbon nanotubes: fundamentals of theory, optics, and transport devices*. New York: Springer Publishers.

Rummeli M.H., E. Borowiak-Palen, T. Gemming, T. Pichler, M. Knupfer, and M. Kalbac. 2005. Novel catalysts, room temperature and the importance of oxygen for the synthesis of single-walled carbon nanotubes. *Nano Letters* 5(7):1209-1215.

Saito, R., M. Fujita, G. Dresselhaus, M.S. Dresselhaus. 1992. Electronic structure of chiral graphene tubules. *Applied Physics Lett*ers 60(18):2204-2207.

Saito Y, M. Okuda, N. Fujimoto, T. Yoshikawa, M. Tomita, T. Hyashi. 1994. Single-wall carbon nanotubes growing rapidly from Ni fine particles formed by arc-evaporation. *Japan Journal of Applied Physics Part 2- Letters* 33:526-529.

Saito, Riichiro, Gene Dresselhaus, and Mildred S. Dresselhaus. 1998. *Physical properties of carbon nanotubes*. London: Imperial College Press.

Satishkumar, B.C., A. Govindaraj, R. Sen, and C.N.R. Rao. 1998. Single-walled nanotubes by the pyrolysis of acetylene-organometallic mixtures. *Chemical Physics Letters* 293:47-52.

Scace R.I and G.A. Slack. 1959. Solubility of carbon in silicon and germanium. *Journal of Chemical Physics* 30(6):1551-1555.

Sen, R., A. Govindaraj, and C.N.R. Rao. 1997. Carbon nanotubes by the metallocene route. *Chemical Physics Letters* 267:276–280.

Seshan, Krishna. 2002. *Handbook of thin film deposition processes and techniques, principles, methods, equipments, and applications*. New York: William Andrew Publishing.

Shanov V., Y.H. Yun, M.J. Schulz. 2006. Synthesis and characterization of carbon nanotube materials. *Journal of the University of Chemical Technology and Metallurgy* 41(4):377-390.

Siegal, M.P., D.L. Overmyer, and P.P. Provencio. 2002. Precise control of multiwall carbon nanotube diameters using thermal chemical vapor deposition. *Applied Physics Letters* 80:2171-2176.

Seidel, R., G.S. Duesberg, E. Unger, A.P. Graham, M. Liebau, and F. Kreupl. 2004. Chemical vapor deposition growth of single-walled carbon nanotubes at 600 °C and a simple growth model. *Journal of Physical Chemistry B* 108:1888-1893.

Snoeck J.-W., G.F. Froment, and M. Fowlest. 1997. Filamentous carbon formation and gasification: thermodynamics, driving force, nucleation, and steady-state growth. *Journal of Catalysis* 169:240-249.

Tans, S. J., M.H. Devoret, H. Dai, A. Thess, R.E. Smalley, L.J. Geerligs, and C. Dekker. 1997. Individual single-wall carbon nanotubes as quantum wires. *Nature* 386:474-477.

Taylor, W.J., T.Y. Tan, U. Gosele. 1993. Carbon precipitation in silicon: why is it so difficult. *Applied Physics Letters* 62(25):3336-3338.

Teo, K.B.K., M. Chhowalla, G.A.J. Amaratunga, W.I. Milne, D.G. Hasko, G. Pirio. 2001. Uniform patterned growth of carbon nanotubes without surface carbon. *Applied Physics Letters* 79:1534-1540.

Thess, A. , R. Lee, P. Nikolaev, H. Dai, P. Petit, J. Robert, C. Xu, Y.H. Lee, S.G. Kim, A.G. Rinzler, D.T. Colbert, G. Scuseria, D. Tomanek, J.E. Fischer, and R.E. Smalley. Crystalline ropes of metallic carbon nanotubes. 1996. *Science* 273:483-487.

Thostenson, E.T., Z. Ren, and T.W. Chou. 2001. Advances in the science and technology of carbon nanotubes and their composites: a review. *Composites science and Technology* 61:1899-1912.

Treffer G., J. Neuhiiuser, G. Marx. 1997. XRD studies of SiC/Si layers on carbon substrates. *Mikrochimica Acta* 125:325-330.

Venegoni, D., P. Serp, R. Feurer, Y. Kihn, C. Vahlas, and P. Kalck. 2002. Parametric study for the growth of carbon nanotubes by catalytic chemical vapor deposition in a fluidized bed reactor *Carbon* 40:1799-1807.

Walker, P.L., F. Rusinko, L.G. Austin. 1959. Gas reactions of carbon. *Advances in Catalysis* 11:133-221.

Wright, A.C., Y. Xiong, N. Maung, S.J. Eichhorn, and R.J. Young. 2003. The influence of the substrate on the growth of carbon nanotubes from nickel clusters: an investigation using STM, FE-SEM, TEM, and Raman spectroscopy. *Material Science and Engineering C* 23:279-283.

Yacaman, M.J., M.M. Yoshida, L. Rendon, and J.G. Santiesteban. 1993. Catalytic growth of carbon microtubules with fullerene structure. *Applied Physics Letters* 62:202-207.

Yi, W., L. Lu, Z. Dian-lin, Z.W. Pan, S.S. Xie. 1999. Linear specific heat of carbon nanotubes. *Physical Review B* 59 (14):9015-9018.

Yudasaka, M., R. Kikuchi, T. Matsui, O. Yoshimasa, and S. Yoshimura. 1995. Specific conditions for Ni catalyzed carbon nanotube growth by chemical vapor deposition. *Applied Physics Letters* 67:2477-2482.

Yudasaka, M., R. Kikuchi, Y. Ohki, E. Ota, and S. Yoshimura. 1997. Behavior of Ni in carbon nanotube nucleation. *Applied Physics Letters* 70:1817-1821.

Zhang, W., Y. Li, W. Kim, D. Wang, and H. Dai. 2002. Imaging as-grown single-walled carbon nanotubes originated from isolated catalytic nanoparticles. *Applied Physics A* 74:325-328.

Zhu, S., C.H. Su, J.C. Cochrane, S. Lehoczky, Y. Cui, and A. Burger. 2002. Growth orientation of carbon nanotubes by thermal chemical vapor deposition. *Journal of Crystal Growth* 234:584-588.